

\mathcal{PT} -symmetric mapping of three states and its implementation on a cloud quantum processor

Yaroslav Balytskyi,¹ Yevgen Kotukh,² Gennady Khalimov,³ Sang-Yoon Chang⁴

¹*Department of Physics and Astronomy, Wayne State University, Detroit, MI, 48201, USA*

²*Department of Information Technologies, Yevhenii
Bereznyak Military Academy, Kyiv, 04050, Ukraine*

³*Department of Information Security, Kharkiv National
University of Radio Electronics, Kharkiv, 61166, Ukraine*

⁴*University of Colorado, Colorado Springs, Colorado, 80918, USA*

(Dated: January 4, 2024)

Abstract

We develop a new \mathcal{PT} -symmetric approach for mapping three pure qubit states, implement it by the dilation method, and demonstrate it with a superconducting quantum processor provided by the IBM Quantum Experience. We derive exact formulas for the population of the post-selected \mathcal{PT} -symmetric subspace and show consistency with the Hermitian case, conservation of average projections on reference vectors, and Quantum Fisher Information. When used for discrimination of $N = 2$ pure states, our algorithm gives an equivalent result to the conventional unambiguous quantum state discrimination. For $N = 3$ states, our approach provides novel properties unavailable in the conventional Hermitian case and can transform an arbitrary set of three quantum states into another arbitrary set of three states at the cost of introducing an inconclusive result. For the QKD three-state protocol, our algorithm has the same error rate as the conventional minimum error, maximum confidence, and maximum mutual information strategies. The proposed method surpasses its Hermitian counterparts in quantum sensing using non-MSE metrics, providing an advantage for precise estimations within specific data space regions and improved robustness to outliers. Applied to quantum database search, our approach yields a notable decrease in circuit depth in comparison to traditional Grover's search algorithm while maintaining the same average number of oracle calls, thereby offering significant advantages for NISQ computers. Additionally, the versatility of our method can be valuable for the discrimination of highly non-symmetric quantum states, and quantum error correction. Our work unlocks new doors for applying \mathcal{PT} -symmetry in quantum communication, computing, and cryptography.

Keywords: \mathcal{PT} -symmetric transformations; Quantum state discrimination; Quantum sensing; Quantum database search; Quantum error correction; IBM Quantum Experience; Quantum key distribution.

I. INTRODUCTION

The problem of identifying information stored in a quantum system is fundamental in quantum computer science, and the simplest option is to use two-dimensional systems or qubits to store quantum information. In classical physics, the state variables of the system are also observables and there is no fundamental limitation on the precision with which they can be determined. By contrast, the quantum observables are represented by operators acting on the vector space, which in the general case do not commute, and the outcome of the measurement has statistical rather than deterministic properties. Quantum systems in different non-orthogonal states are impossible to perfectly distinguish even when arbitrary large but finite number of samples for the measurements are available [1–6]. In other words, no test exists which allows to guess correctly all of the time and this fact is highlighted by the quantum Chernoff bound [7].

Quantum state discrimination involves two parties who agree on a set of allowed states in which the system can be, and their prior probabilities of occurrence. A measurement can obtain only a finite amount of information, and thus this set must be finite. Alice prepares a state from this set and sends it to Bob, who must determine it using the appropriate measurement. Quantum state discrimination has a number of important applications. In particular, it is strongly linked to a dimension witness of quantum systems [8] and represents an operational interpretation of conditional mutual entropy [9]. The quantum key distribution (QKD) security is based on the hardness of quantum state discrimination and on the no-cloning theorem [10]. The search over an unstructured database can be mapped to the discrimination of the states exponentially close to each other [11].

Quantum state discrimination is difficult apart from the $N = 2$ case, and the existing strategies for quantum state discrimination can be classified into the minimum error discrimination [2], unambiguous discrimination [12, 13], and maximum confidence discrimination [14], each with its own advantages and drawbacks. The minimum error discrimination solution was obtained for the states possessing particular symmetries such as “geometrically uniform” states [15], and mirror-symmetric states [16]. In the general case of $N = 3$ states, the minimum error discrimination solution for pure qubit states was obtained in [17, 18]. The analytic solution for mixed qubit states without necessary and sufficient conditions was obtained in [19], and the complete analysis was performed in [20]. In the general case, however, the solution requires intricate computation. Unambiguous state discrimination can be achieved only for linearly independent states [21], and therefore is not possible for $N = 3$ qubit states.

Meanwhile, recent developments in \mathcal{PT} -symmetric quantum mechanics [22–24], where the condition of Hermiticity is replaced by the condition of \mathcal{PT} -symmetry, provide new opportu-

nities for the quantum information science, that are not available in the usual Hermitian case. Such theories possess an additional degree of freedom represented by the α parameter, and in the limit $\alpha \rightarrow 0$, the intersection of \mathcal{PT} -symmetric and Hermitian cases are real symmetric Hamiltonians [25]. At certain values of the α parameter, the degeneracies occur, known as exceptional points, which correspond to coalescing eigenvectors and eigenvalues [26, 27].

These points can be used in multiple applications. First, in the \mathcal{PT} -symmetric system, the time of quantum evolution may approach *theoretically zero* in the vicinity of the exceptional point, while in the Hermitian one, a finite time is needed. This effect was demonstrated both theoretically [28] and experimentally [29]. Second, it was used for enhanced sensing [30–35], and it has been shown that \mathcal{PT} -symmetric sensors are 8.856 times superior to Hermitian ones [36]. Moreover, \mathcal{PT} -symmetric operations increase the quantum Fisher information needed to increase the accuracy of quantum parameter estimation [37, 38], which in turn was used for the Bayesian parameter estimation [39–41]. The existence of exceptional points was demonstrated in multiple classical systems as well [42–50], and they found applications in laser mode management [51–53], and topological mode transfer [54–57]. For $N = 2$ states, the \mathcal{PT} -symmetric discrimination was developed in [58], and the focus of our work is an extension of this method for $N = 3$ states. For the first time, we derive exact expressions for the population of postselected space, enabling us to pinpoint scenarios in which \mathcal{PT} -symmetric systems outperform their Hermitian counterparts.

II. RESULTS

First, we provide a necessary background on \mathcal{PT} symmetry in Section III. In Section IV, we develop a \mathcal{PT} symmetric approach for the $N = 3$ pure quantum states discrimination, which consists of two stages of \mathcal{PT} symmetric evolution. In the first one, two of the three states are made mutually orthogonal in terms of the Hermitian scalar product. The second stage enables the transformation of a given set of three arbitrary states into another set of states as required. In the limiting case as α approaches $\pm\frac{\pi}{2}$, near the exceptional point, the geometry of the postselected space closely resembles that of a two-state scenario. Our initial findings regarding the \mathcal{PT} -symmetric subsystem [59] were validated through experiments conducted on an optical setup [60] (see Section III and Ref. [38] there for further information). In comparison to prior studies where numerical computations and experimentation were employed [61, 62] to embed \mathcal{PT} -symmetric subsystem into a Hermitian Hamiltonian, in Section V, we derive exact expressions for the population of the postselected \mathcal{PT} -symmetric subspace and show that for the case of $N = 2$ states, the proposed method is analogous to conventional unambiguous quantum state discrimination [13]. In Section VI, we provide

a comparison between our theoretical model and the results of the runs on IBM Quantum Experience. The details of implementation are provided in Methods. In Section VII, we demonstrate that our algorithm has an identical error rate when employed to attack the trine state QKD protocol as compared to minimum error, maximum confidence, and maximum mutual information strategies. We demonstrate consistency with the Hermitian case, conservation of average projection on reference vectors, and Quantum Fisher Information (QFI). In Section VIII, we discuss applications of our method where it outperforms its Hermitian counterparts, in particular, quantum sensing with non-MSE loss performance functions and paralleled Grover search algorithm. We show that our algorithm uses the same average number of oracle calls as paralleled Grover’s search algorithm, but allows for a significant reduction in scheme *depth*, which has significant implications, especially in light of the NIST restrictions on the circuit depth used for quantum attacks. We hypothesize that the ability of our method to transform a mixture of three arbitrary states into a standardized set of three stabilizer states has significant implications for quantum error correction and the discrimination of states with highly asymmetric geometries. We present our conclusions and outline future work in Section IX.

III. BACKGROUND ON \mathcal{PT} SYMMETRY

In order to have a complete description of the physical system, the energy eigenvalues must be real-valued. Complex energies are often used to describe dissipative phenomena when the probability of finding a particle decreases over time. The decaying particle, however, does not vanish but transforms into other particles, and therefore such a description is incomplete. The condition of reality of the spectra can be achieved by constraining the Hamiltonian to be Hermitian $H = H^\dagger$. Nevertheless, this condition is not necessary and can be replaced by a condition of an unbroken \mathcal{PT} -symmetry [22–24] which guarantees that all eigenvalues of the Hamiltonian are real. Additionally, it provides an extra degree of freedom not available in the Hermitian case which we describe further.

The Hamiltonian is \mathcal{PT} -symmetric if it satisfies the condition $\mathcal{H} = \mathcal{H}^{\mathcal{PT}}$. The signs of the quantum mechanical coordinate and momentum, \hat{x} and \hat{p} , are changed by the parity operator \mathcal{P} as $\mathcal{P}\hat{x}\mathcal{P} = -\hat{x}$, $\mathcal{P}\hat{p}\mathcal{P} = -\hat{p}$, and for the case of qubit, up to a unitary transformation, is given by [28]:

$$\mathcal{P} = \begin{pmatrix} 0 & 1 \\ 1 & 0 \end{pmatrix} \quad (1)$$

Time-reversal operator \mathcal{T} changes the signs of the imaginary unit and the momentum operator as $\mathcal{T}i\mathcal{T} = -i$ and $\mathcal{T}\hat{p}\mathcal{T} = -\hat{p}$. The \mathcal{PT} operator is a combination of \mathcal{P} and \mathcal{T} . For the

case of qubit, the most general \mathcal{PT} -symmetric depends on three real parameters r , s and β as [58]:

$$\mathcal{H} = \mathcal{H}^{\mathcal{PT}} = \begin{pmatrix} re^{i\beta} & s \\ s & re^{-i\beta} \end{pmatrix} \quad (2)$$

The \mathcal{PT} -symmetric Hamiltonian is called to be possessing an unbroken \mathcal{PT} symmetry if each of its eigenfunctions is also an eigenfunction of the \mathcal{PT} operator. This condition guarantees that all energy eigenvalues are real [63, 64]. Additionally, this condition provides an extra \mathcal{C} operator which is represented by the sum of all eigenfunctions of the \mathcal{PT} -symmetric Hamiltonian, Eqn. 2:

$$\mathcal{H}\psi_n(x) = E_n\psi_n(x), \quad \mathcal{C}(x, y) = \sum_{n=1}^2 \psi_n(x)\psi_n(y) \quad (3)$$

For the qubit case, it takes the form:

$$\mathcal{C} = \frac{1}{\cos(\alpha)} \begin{pmatrix} i \sin(\alpha) & 1 \\ 1 & -i \sin(\alpha) \end{pmatrix}, \quad (4)$$

with α being expressed as $\sin(\alpha) = \frac{r}{s} \sin(\beta)$. As a result, the set of commuting operators in the \mathcal{PT} -symmetric theory is bigger in comparison with the Hermitian case, $[\mathcal{C}, \mathcal{H}] = 0$ and $[\mathcal{C}, \mathcal{PT}] = 0$. The ket vector both in the Hermitian and \mathcal{PT} -symmetric cases has the same form:

$$|\psi\rangle = \begin{pmatrix} \cos\left(\frac{\theta}{2}\right) \\ e^{i\phi} \sin\left(\frac{\theta}{2}\right) \end{pmatrix}, \quad (5)$$

with θ and ϕ being the meridian and parallel of the Bloch sphere of the qubit respectively. The difference is in the scalar product which is fixed in the Hermitian case but in the \mathcal{PT} -symmetric one is *defined* by the \mathcal{C} operator given in Eqn. 4 as $(\langle\psi|\rangle)_{\mathcal{CPT}} = (\mathcal{CPT}|\psi\rangle)^T$, $(\langle\mu|\nu\rangle)_{\mathcal{CPT}} = (\mathcal{CPT}|\mu\rangle)^T \cdot |\nu\rangle$, here the over-script T is matrix transposition and the \mathcal{CPT} operation is a combination of \mathcal{C} and \mathcal{PT} operators which we defined previously. The limit $\alpha \rightarrow 0$ recovers the regular Hermitian case since $\lim_{\alpha \rightarrow 0} (\mathcal{C}) = \mathcal{P}$.

This property was used for $N = 2$ state discrimination [46] to manipulate the angle between state vectors effectively converting them into orthogonal ones. The no-cloning theorem [10] still applies both for the Hermitian and \mathcal{PT} -symmetric case since this conversion happens at the cost of introducing an inconclusive outcome meaning that the \mathcal{PT} -symmetric part of the total wave-function of the system has a norm less than one, in the general case.

For two non-orthogonal states on the $\phi = -\frac{\pi}{2}$ parallel:

$$|\psi_{1,2}\rangle = \begin{pmatrix} \cos\left(\frac{\pi \mp 2\sigma}{4}\right) \\ -i \sin\left(\frac{\pi \mp 2\sigma}{4}\right) \end{pmatrix}, \quad (6)$$

this conversion may be obtained by two possible *Solutions*:

- *Solution 1: zeroing the CPT product $(\text{CPT}|\psi_1\rangle)^T \cdot |\psi_2\rangle = 0$ by setting the Hamiltonian in Eqn. 2 to make $\sin(\alpha) = \frac{r}{s} \sin(\beta) = \cos(\sigma)$.*
- *Solution 2: performing \mathcal{PT} -symmetric Hamiltonian evolution to $(\langle\psi_1|\psi_2\rangle)_{\text{Hermitian}} = 0$ for a time τ_{Perp} :*

$$\sin^2(\omega\tau_{\text{Perp}}) = \frac{\cos^2(\alpha) \cos(\sigma)}{2 \sin(\alpha) (1 - \sin(\alpha) \cos(\sigma))}, \quad \omega = \sqrt{s^2 - r^2 \sin^2(\beta)}, \quad (7)$$

effectively modifying the metrics as:

$$\cos^2(\alpha) e^{+i\mathcal{H}^\dagger t} e^{-i\mathcal{H}t} = \begin{pmatrix} \cos^2(\omega t - \alpha) + \sin^2(\omega t) & -2i \sin^2(\omega t) \sin(\alpha) \\ 2i \sin^2(\omega t) \sin(\alpha) & \cos^2(\omega t + \alpha) + \sin^2(\omega t) \end{pmatrix} \quad (8)$$

In contrast to the Hermitian case, in \mathcal{PT} -symmetric dynamics, the states $|0\rangle$ and $|1\rangle$ exhibit an angular separation of $\pi - 2|\alpha|$ [28]. As the system approaches the exceptional point in the limit $\alpha \rightarrow \pm\frac{\pi}{2}$, these states merge.

In Section V, we show that for the case of two states, $N = 2$, and minimal value of α allowed by Eqn. 7, this approach is equivalent to an unambiguous quantum state discrimination [13]. In Section IV, we extend the \mathcal{PT} -symmetric approach to three states, $N = 3$, through a double \mathcal{PT} -symmetric evolution. By leveraging the properties of exceptional points, we demonstrate novel features not present in the Hermitian case.

IV. SCHEME FOR \mathcal{PT} -SYMMETRIC TRANSFORMATION OF $N = 3$ STATES

Our approach consists of three steps and can be summarized as:

- *Step 1: evolve two of the states, $|\psi_1\rangle$ and $|\psi_2\rangle$, into the orthogonal ones in terms of the Hermitian scalar product, $(\langle\psi_1|\psi_2\rangle)_{\text{Hermitian}} = 0$, by applying the first \mathcal{PT} -symmetric evolution.*

- *Step 2*: By applying a unitary rotation, convert these states into $|\psi_{1,2}\rangle \rightarrow \frac{1}{\sqrt{2}} \begin{pmatrix} 1 \\ \pm i \end{pmatrix}$.

In these positions, they remain orthogonal under the \mathcal{PT} operations with an arbitrary value of α parameter, and we use it to adjust a relative angle to the third state.

- *Step 3*: Perform a second \mathcal{PT} -symmetric evolution to adjust the angle between $|\psi_{1,2}\rangle$ and $|\psi_3\rangle$, and perform the projective measurement in \mathcal{PT} -symmetric subsystem.

Without loss of generality, an arbitrary set of three states $|\psi_i\rangle = \begin{pmatrix} \cos(\frac{\theta_i}{2}) \\ e^{i\phi_i} \sin(\frac{\theta_i}{2}) \end{pmatrix}$, $i \in [1, 3]$ can be adjusted to the following positions by unitary rotations provided in Eqn. 88 in Methods:

$$|\psi_{1,2}\rangle \rightarrow \begin{pmatrix} \cos(\frac{\pi \mp 2\sigma}{4}) \\ -i \sin(\frac{\pi \mp 2\sigma}{4}) \end{pmatrix}, |\psi_3\rangle \rightarrow \begin{pmatrix} \cos(\frac{\mu}{2}) \\ e^{i\nu} \sin(\frac{\mu}{2}) \end{pmatrix}, \quad (9)$$

and σ , μ and ν parameters in the following equations.

In *Step 1*, we use \mathcal{PT} -symmetric evolution controlled by the Hamiltonian in Eqn. 2, and perform it for a time τ_{Perp} in Eqn. 7. As a result, the first pair of states takes the form:

$$|\psi_1\rangle \rightarrow \begin{pmatrix} \cos(\frac{\delta}{2}) \\ -i \sin(\frac{\delta}{2}) \end{pmatrix}, |\psi_2\rangle \rightarrow \begin{pmatrix} \sin(\frac{\delta}{2}) \\ i \cos(\frac{\delta}{2}) \end{pmatrix}, \quad (10)$$

with the δ parameter provided by the Eqn. 11 and 12:

$$\cos\left(\frac{\delta}{2}\right) = \frac{\cos(\omega\tau_{Perp} - \alpha) \cos\left(\frac{\pi - 2\sigma}{4}\right) - \sin(\omega\tau_{Perp}) \sin\left(\frac{\pi - 2\sigma}{4}\right)}{\sqrt{\mathcal{V}}}, \quad (11)$$

$$\begin{aligned} \mathcal{V} &= 1 - \cos(2\omega\tau_{Perp}) \sin^2(\alpha) \\ &+ 2 \sin(\omega\tau_{Perp}) \sin(\alpha) (\cos(\omega\tau_{Perp}) \cos(\alpha) \sin(\sigma) - \sin(\omega\tau_{Perp}) \cos(\sigma)) \end{aligned} \quad (12)$$

In *Step 2*, we apply the following gate with the χ parameter given by Eqn. 97 in Methods:

$$\mathcal{W} = \frac{1}{\sqrt{2}} \begin{pmatrix} 1 & i \\ i & 1 \end{pmatrix} \cdot \begin{pmatrix} 1 & 0 \\ 0 & ie^{-i\chi} \end{pmatrix} \cdot \begin{pmatrix} \cos(\frac{\delta}{2}) & i \sin(\frac{\delta}{2}) \\ i \sin(\frac{\delta}{2}) & \cos(\frac{\delta}{2}) \end{pmatrix}, \quad (13)$$

$$|\chi_{(1,2,3)}\rangle = \mathcal{W} |\psi_{(1,2,3)}\rangle \quad (14)$$

The resulting states take the following form, with $\rho = \xi + \frac{\pi}{2}$ and ξ provided in Eqn. 97:

$$|\chi_1\rangle = \frac{1}{\sqrt{2}} \begin{pmatrix} 1 \\ i \end{pmatrix}, |\chi_2\rangle = \frac{1}{\sqrt{2}} \begin{pmatrix} 1 \\ -i \end{pmatrix}, |\chi_3\rangle = \begin{pmatrix} \cos(\frac{\rho}{2}) \\ i \sin(\frac{\rho}{2}) \end{pmatrix} \quad (15)$$

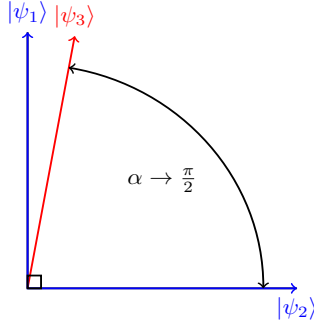


Figure 1. Geometry of post-selected space for $\alpha \rightarrow \frac{\pi}{2}$.

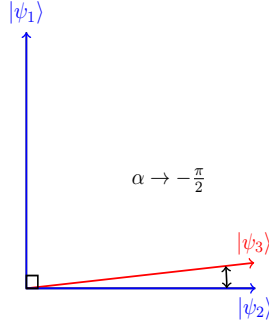


Figure 2. Geometry of post-selected space for $\alpha \rightarrow -\frac{\pi}{2}$.

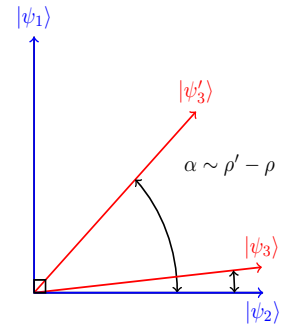


Figure 3. Geometry modification by α variation.

We proceed to the second \mathcal{PT} -symmetric evolution constituting *Step 3*. After *Step 2*, the first two states are orthogonal, and we can adjust the relative angle to the third state. For completeness, we consider both Hermitian and \mathcal{CPT} measurements.

A. *Step 3* by Hermitian measurement

We apply the second \mathcal{PT} -symmetric evolution by the Hamiltonian in Eqn. 2 for a time τ^{II} , and the relative angles between the evolved states κ_{12} , κ_{13} and κ_{23} are given by:

$$\begin{cases} \cos_{\mathcal{PT}}^2(\kappa_{12}) = \frac{2 \tan^2(\alpha) \sin^2(2\omega\tau^{II})}{1 + \sec^2(\alpha) - \tan^2(\alpha) \cos(4\omega\tau^{II})} \\ \cos_{\mathcal{PT}}^2(\kappa_{13}, \kappa_{23}) = \frac{(\sqrt{2} \sin(\frac{\pi \pm 2\rho}{4}) [(1 \pm 2 \sin(\alpha)) \sin^2(\omega\tau^{II}) + \cos^2(\omega\tau^{II} + \alpha)] + \sin(2\alpha) \cos(\frac{\rho}{2}) \sin(2\omega\tau^{II}))^2}{2((1 \pm \sin(\alpha))^2 \sin^2(\omega\tau^{II}) + \cos^2(\alpha) \cos^2(\omega\tau^{II})) (\sin^2(\omega\tau^{II})(1 + 2 \sin(\alpha) \sin(\rho)) - \sin(2\alpha) \sin^2(\frac{\rho}{2}) \sin(2\omega\tau^{II}) + \cos^2(\omega\tau^{II} - \alpha))} \end{cases} \quad (16)$$

By the subscript \mathcal{PT} in $\cos_{\mathcal{PT}}^2$, we mean the effective cosine squared in \mathcal{PT} -symmetric subspace after postselection. We derive exact expressions for the probability of postselection the next Section V. After the time $\tau^{II} = \frac{\pi}{2\omega}$, these expressions take the form:

$$\begin{cases} \cos_{\mathcal{PT}}^2(\kappa_{12}) = 0 \\ \cos_{\mathcal{PT}}^2(\kappa_{13}, \kappa_{23}) = \frac{(1 \pm \sin(\alpha))^2 (1 \pm \sin(\rho))}{3 + 4 \sin(\alpha) \sin(\rho) - \cos(2\alpha)} \end{cases} \quad (17)$$

In the limit $\alpha \rightarrow \frac{\pi}{2}$ we obtain:

$$\cos_{\mathcal{PT}}^2(\kappa_{13}) = 1 - \frac{(1 - \sin(\rho)) \left(\frac{\pi}{2} - \alpha\right)^4}{16 (1 + \sin(\rho))} + O\left(\left(\frac{\pi}{2} - \alpha\right)^5\right), \quad (18)$$

$$\cos_{\mathcal{PT}}^2(\kappa_{23}) = \frac{(1 - \sin(\rho)) \left(\frac{\pi}{2} - \alpha\right)^4}{16(1 + \sin(\rho))} + O\left(\left(\frac{\pi}{2} - \alpha\right)^5\right), \quad (19)$$

and for $\alpha \rightarrow -\frac{\pi}{2}$ we have:

$$\cos_{\mathcal{PT}}^2(\kappa_{13}) = \frac{(1 + \sin(\rho)) \left(\frac{\pi}{2} + \alpha\right)^4}{16(1 - \sin(\rho))} + O\left(\left(\frac{\pi}{2} + \alpha\right)^5\right), \quad (20)$$

$$\cos_{\mathcal{PT}}^2(\kappa_{23}) = 1 - \frac{(1 + \sin(\rho)) \left(\frac{\pi}{2} + \alpha\right)^4}{16(1 - \sin(\rho))} + O\left(\left(\frac{\pi}{2} + \alpha\right)^5\right) \quad (21)$$

The corresponding geometry of the states in these limits is shown in Fig. 1 and Fig. 2. These results *apparently* seem contradictory to the well-known impossibility of unambiguous discrimination of linearly dependent states [21]. However, such \mathcal{PT} -symmetric transformation inevitably involves postselection, and in the next Section V, we show that changing the angles in the \mathcal{PT} -symmetric subspace happens at the cost of reduction of postselection probability. Considering the probability of postselection, these results align with those presented in [21].

As shown in Eqn. 15, in the general case, an arbitrary set of three states can be reduced to the states in Eqn. 15 by \mathcal{PT} -symmetric transformations. Thus an arbitrary set of three states is uniquely characterized by its ρ value, up to the initial unitary transformation in Methods. Therefore, the parameter α can be employed to convert a set of three states characterized by the parameter ρ into another set of three states corresponding to the parameter ρ' . This can be done by setting the value of α to be:

$$\sin(\alpha) = \min\left\{\frac{\cos\left(\frac{\rho+\rho'}{2}\right)}{\sin\left(\frac{\rho'-\rho}{2}\right)}, \frac{\sin\left(\frac{\rho'-\rho}{2}\right)}{\cos\left(\frac{\rho+\rho'}{2}\right)}\right\}, \quad (22)$$

depending on the values of ρ and ρ' to ensure that $|\sin(\alpha)| \leq 1$, as illustrated in Fig. 3. By running *Steps 1* and *2* backward, one can transform the second set of states to the first one. As we discuss in Section V, when postselection probability is taken into account, this does not lead to the reduction of error rate in comparison with conventional Hermitian approaches. However, this property may be useful for the discrimination of states with highly asymmetric geometries as we discuss in Section VIII.

As an example, one can achieve *effective* mirror-symmetric geometry of postselected states corresponding to $\rho' = 0$, when $\cos_{\mathcal{PT}}^2(\kappa_{13}) = \cos_{\mathcal{PT}}^2(\kappa_{23}) = \frac{1}{2}$ in Eqn.17, by choosing:

$$\sin(\alpha) = \left\{ -\cot\left(\frac{\rho}{2}\right), -\tan\left(\frac{\rho}{2}\right) \right\} \quad (23)$$

After application of S gate:

$$S = \begin{pmatrix} 1 & 0 \\ 0 & i \end{pmatrix}, \quad (24)$$

this set of states is transformed to $|+\rangle$, $|-\rangle$, and $|0\rangle$. These are stabilizer states [65], and we discuss possible implications of this for quantum error correction in Section VIII. Finally, as we show in Section V, even though the *effective* geometry of postselected states is mirror-symmetric, the postselection changes the prior probabilities, so even though the effective angles $\kappa_{13} = \kappa_{23} = \frac{\pi}{4}$ are the same, prior probabilities of $|\psi_1\rangle$ and $|\psi_2\rangle$ are different in the general case.

B. Step 3 \mathcal{CPT} measurement

The same result can be achieved using the \mathcal{CPT} measurement, since for an arbitrary α the states $|\psi_1\rangle$ and $|\psi_2\rangle$ are mutually orthogonal:

$$(\langle\psi_1|\psi_2\rangle)_{\mathcal{CPT}} = 0; (\langle\psi_{1,2}|)_{\mathcal{CPT}} = \frac{(1 \pm \sin(\alpha))}{\sqrt{2} \cos(\alpha)} (1, \mp i) \quad (25)$$

This allows to use the value of α to adjust the relative angles with the third state κ_{13} and κ_{23} :

$$\begin{cases} \cos_{\mathcal{PT}}^2(\kappa_{12}) = 0 \\ \cos_{\mathcal{PT}}^2(\kappa_{13}, \kappa_{23}) = \frac{(1 \pm \sin(\alpha))(1 \pm \sin(\rho))}{2(1 + \sin(\alpha) \sin(\rho))} \end{cases}, \quad (26)$$

and for $\alpha \rightarrow \frac{\pi}{2}$ represented in Fig. 1:

$$\cos_{\mathcal{PT}}^2(\kappa_{13}) = 1 - \frac{\left(\frac{\pi}{2} - \alpha\right)^2 (1 - \sin(\rho))}{4(1 + \sin(\rho))} + O\left(\left(\frac{\pi}{2} - \alpha\right)^3\right), \quad (27)$$

$$\cos_{\mathcal{PT}}^2(\kappa_{23}) = \frac{\left(\alpha - \frac{\pi}{2}\right)^2 (1 - \sin(\rho))}{4(1 + \sin(\rho))} + O\left(\left(\alpha - \frac{\pi}{2}\right)^3\right) \quad (28)$$

In the limit $\alpha \rightarrow -\frac{\pi}{2}$ corresponding to Fig. 2:

$$\cos_{\mathcal{PT}}^2(\kappa_{13}) = \frac{\left(\frac{\pi}{2} + \alpha\right)^2 (1 + \sin(\rho))}{4(1 - \sin(\rho))} + O\left(\left(\frac{\pi}{2} + \alpha\right)^3\right), \quad (29)$$

$$\cos_{\mathcal{PT}}^2(\kappa_{23}) = 1 - \frac{\left(\frac{\pi}{2} + \alpha\right)^2 (1 + \sin(\rho))}{4(1 - \sin(\rho))} + O\left(\left(\frac{\pi}{2} + \alpha\right)^3\right) \quad (30)$$

Analogously to the Hermitian case, the \mathcal{CPT} projection operators can be introduced which are the \mathcal{CPT} observables:

$$\hat{P}_{1,2} = \left(\frac{|\psi_{1,2}\rangle\langle\psi_{1,2}|}{\langle\psi_{1,2}|\psi_{1,2}\rangle} \right)_{\mathcal{CPT}} = \frac{1}{2} \begin{pmatrix} 1 & \mp i \\ \pm i & 1 \end{pmatrix}, [\mathcal{CPT}, \hat{P}_{1,2}] = 0 \quad (31)$$

Similarly to the Hermitian case in Eqn. 22, it is possible to transform the states $\rho \rightarrow \rho'$ by choosing:

$$\sin(\alpha) = \frac{\sin(\rho') - \sin(\rho)}{1 - \sin(\rho')\sin(\rho)}, \quad (32)$$

and when $\alpha = -\rho$ three states are reduced to effectively mirror-symmetric corresponding to $\rho' = 0$, as illustrated in Fig. 3.

Since the \mathcal{PT} -symmetric transformations involve postselection, in order for one to have a fair comparison of their performance with their Hermitian counterparts, one needs to compute the probability of successful postselection. Unlike prior studies where numerical computations were employed [61, 62], in the next Section V, we formulate precise expressions for the probability of achieving a definitive outcome following \mathcal{PT} -symmetric evolution.

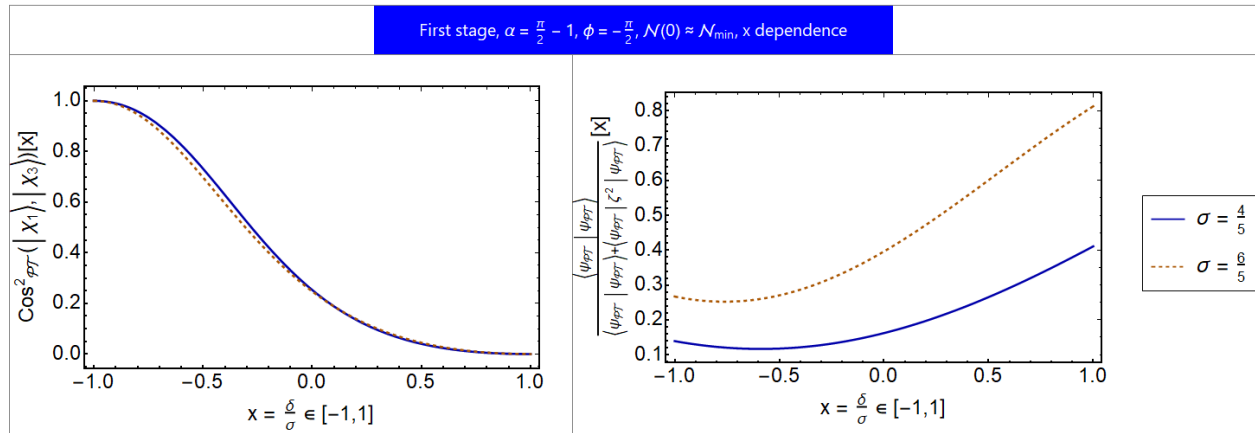


Figure 4. $\cos^2_{\mathcal{PT}}$ in \mathcal{PT} -symmetric subsystem and population of postselected space corresponding to the state $|\psi_3\rangle$.

V. EMBEDDING BY THE DILATION METHOD

We implement the \mathcal{PT} -symmetric Hamiltonian evolution by extending the original qubit with ancilla and employing Neumark's theorem [66], similarly to [61, 62]. The combined

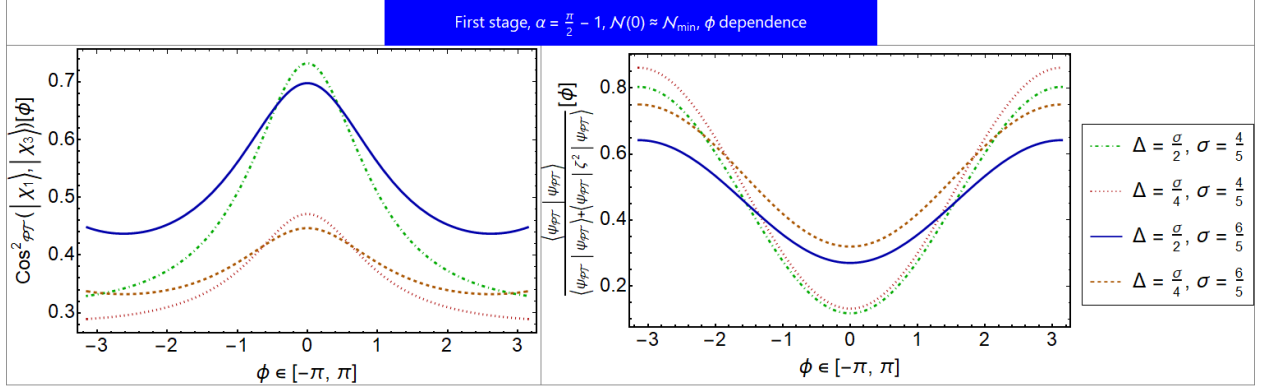


Figure 5. $\text{cos}^2_{\mathcal{PT}}$ in \mathcal{PT} -symmetric subsystem and population of postselected space corresponding to the state $|\psi'_3\rangle$.

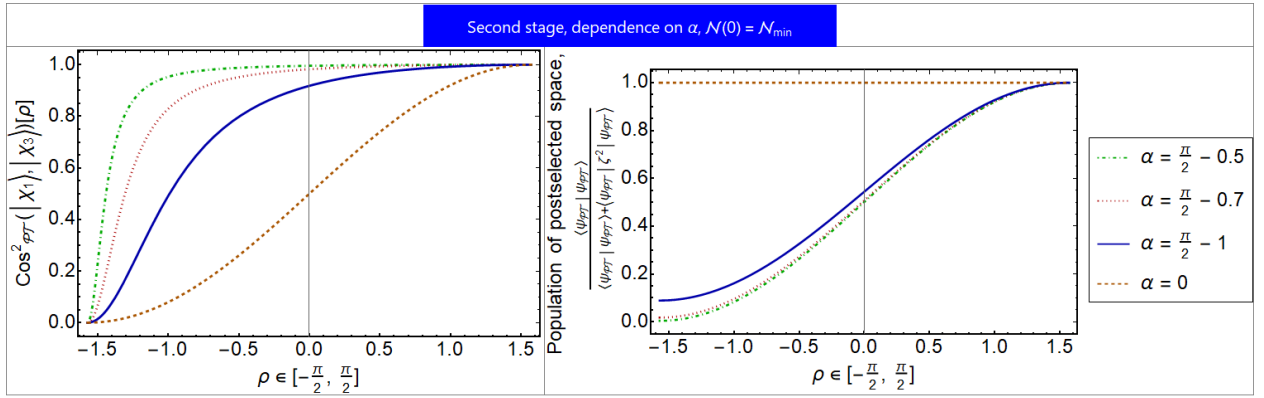


Figure 6. *Stage 2* as α approaches the exceptional point $\frac{\pi}{2}$.

ancilla-qubit wave function $|\Psi_{combined}(t)\rangle$ with the \mathcal{PT} -symmetric subspace $|\psi_{\mathcal{PT}}(t)\rangle$ is:

$$|\Psi_{combined}(t)\rangle = |\psi_{\mathcal{PT}}(t)\rangle |0\rangle_{ancilla} + \zeta(t) |\psi_{\mathcal{PT}}(t)\rangle |1\rangle_{ancilla}, \quad (33)$$

where operator $\zeta(t) = \zeta^\dagger(t) = (\mathcal{N}(t) - \hat{1})^{\frac{1}{2}}$ must maintain all its eigenvalues to be real, and the initial value $\mathcal{N}(0)$ must be correspondingly chosen in order to ensure it, with:

$$\mathcal{N}(t) = T \exp \left[-i \int_0^t d\tau' \mathcal{H}_q^\dagger(\tau') \right] \mathcal{N}(0) \tilde{T} \exp \left[i \int_0^t d\tau' \mathcal{H}(\tau') \right], \quad (34)$$

where T and \tilde{T} are the time and anti-time-ordering operators, respectively.

Further in the text, we perform analytical computations to find the minimal value of $\mathcal{N}(0)$ that maximizes the probability of the conclusive outcome. Thus, unlike numerical

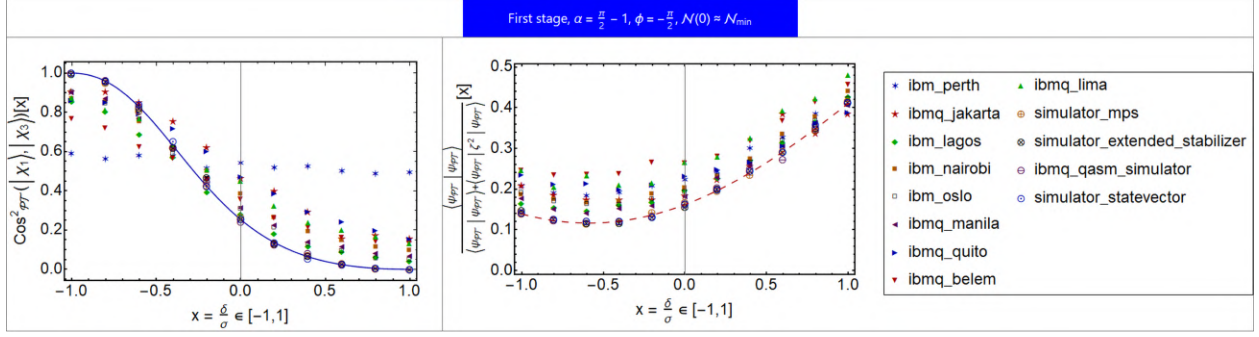


Figure 7. *Stage 1* with $\sigma = \frac{4}{5}$ corresponding to the probe state $|\psi_3\rangle$ in Eqn. 58.

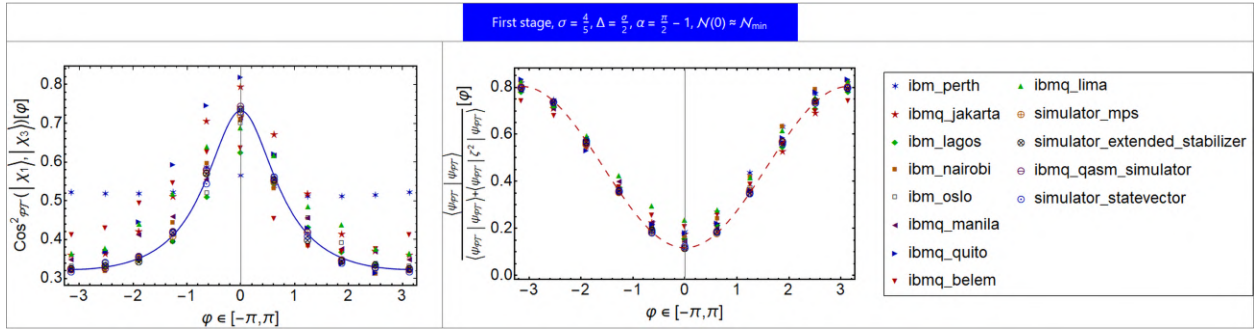


Figure 8. *Stage 1* with $\sigma = \frac{4}{5}$ and $\Delta = \frac{\sigma}{2}$ corresponding to the probe state $|\psi'_3\rangle$ in Eqn. 58.

computations in [61, 62], for both the first and second stages of \mathcal{PT} -symmetric evolution, we find the population of postselected space *exactly* as:

$$\mathcal{D} = \frac{\langle \psi_{\mathcal{PT}}(t) | \psi_{\mathcal{PT}}(t) \rangle}{\langle \psi_{\mathcal{PT}}(t) | \psi_{\mathcal{PT}}(t) \rangle + \langle \psi_{\mathcal{PT}}(t) | \zeta^2(t) | \psi_{\mathcal{PT}}(t) \rangle}, \quad (35)$$

A. First stage

As was shown experimentally in [60], at the critical value, \mathcal{PT} -symmetric quantum state discrimination is equivalent to the optimal unambiguous state discrimination in Hermitian systems [13]. Our present work offers the analytical derivation that was lacking in the prior literature.

First, the smallest value of α in Eqn. 7 allowing to perform \mathcal{PT} -symmetric evolution corresponding to $\sin^2(\omega\tau_{Perp}) = 1$ is given by:

$$\sin(\alpha) = (1 - \sin(\sigma)) \sec(\sigma) \quad (36)$$

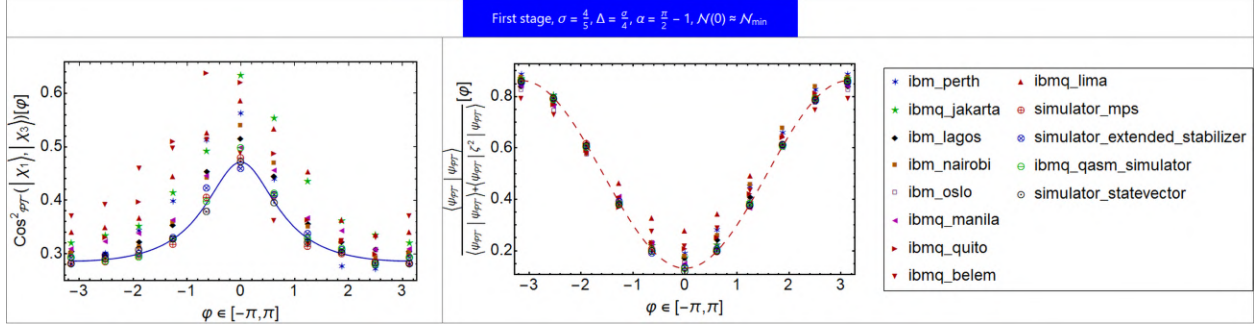


Figure 9. *Stage 1* with $\sigma = \frac{4}{5}$ and $\Delta = \frac{\sigma}{4}$ corresponding to the probe state $|\psi'_3\rangle$ in Eqn. 58.

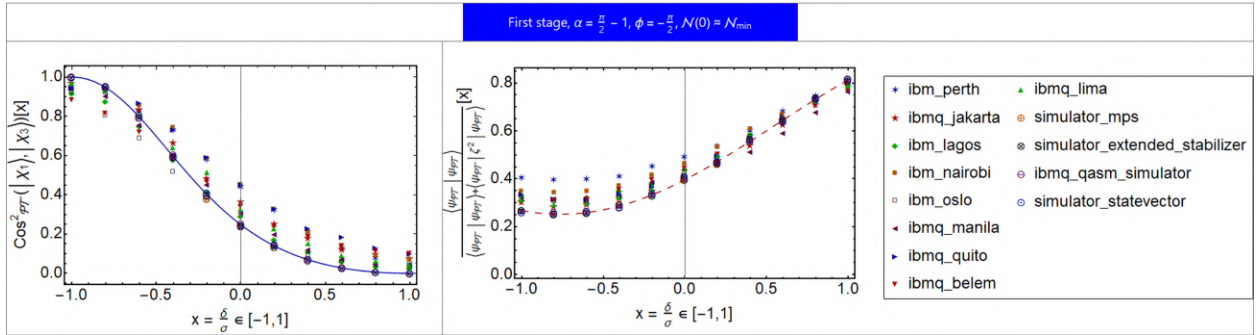


Figure 10. *Stage 1* with $\sigma = \frac{6}{5}$ corresponding to the probe state $|\psi_3\rangle$ in Eqn. 58.

For added convenience, alongside the pair of reference vectors in Eqn. 6, we introduce the vector situated between them, aligning along the same parallel of the Bloch sphere:

$$|\psi_m\rangle = \begin{pmatrix} \cos\left(\frac{\pi+2m}{4}\right) \\ -i \sin\left(\frac{\pi+2m}{4}\right) \end{pmatrix} \quad (37)$$

The resulting $\cos^2_{\mathcal{PT}}(|\psi_m\rangle, |\psi_1\rangle)$ in the postselected subspace turns out to be the same as computed by the \mathcal{CPT} scalar product [39]:

$$\cos^2_{\mathcal{PT}}(|\psi_m\rangle, |\psi_1\rangle) = \frac{1 - \cos(m - \sigma)}{2(1 - \cos(m) \cos(\sigma))} \quad (38)$$

By explicitly computing the eigenvalues of $\zeta(t)$, we find that the requirement that they remain real throughout the evolution simplifies to the condition:

$$\mathcal{N}(0) \cot\left(\frac{\sigma}{2}\right) - 1 \geq 0 \quad \& \quad \mathcal{N}(0) \tan\left(\frac{\sigma}{2}\right) - 1 \geq 0, \quad (39)$$

and thus:

$$\mathcal{N}(0) = \max\left\{ \tan\left(\frac{\sigma}{2}\right), \cot\left(\frac{\sigma}{2}\right) \right\} \quad (40)$$

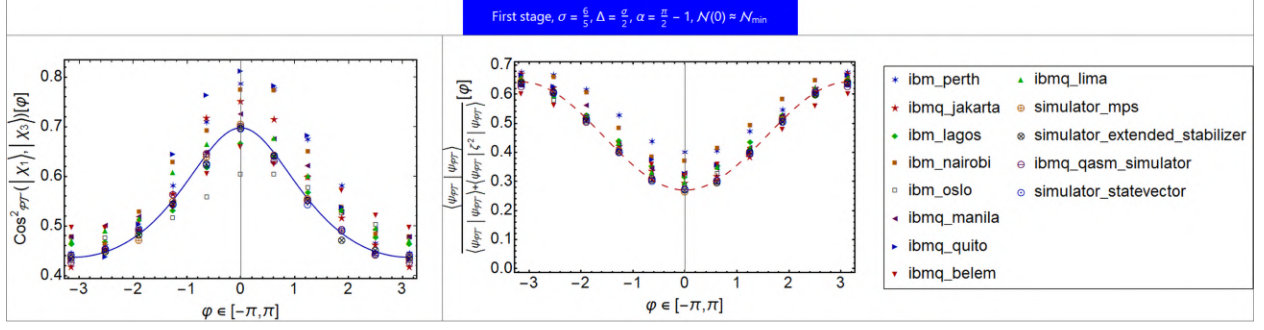


Figure 11. *Stage 1* with $\sigma = \frac{6}{5}$ and $\Delta = \frac{\sigma}{2}$ corresponding to the probe state $|\psi'_3\rangle$ in Eqn. 58.

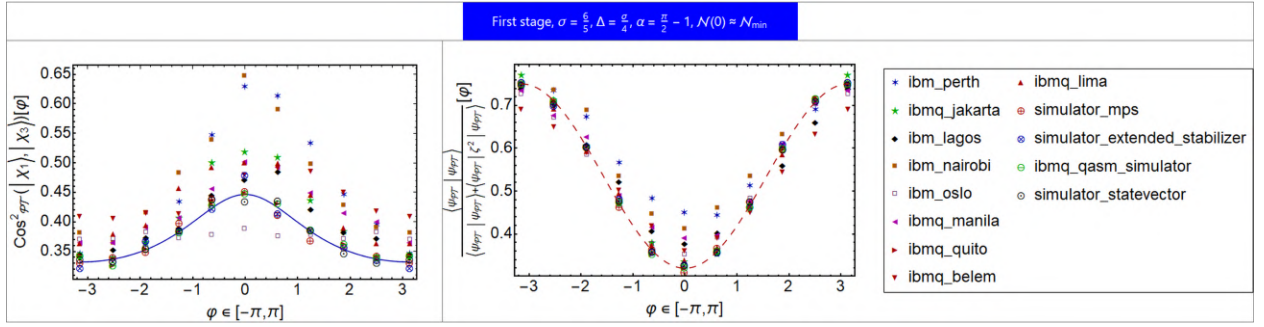


Figure 12. *Stage 1* with $\sigma = \frac{6}{5}$ and $\Delta = \frac{\sigma}{4}$ corresponding to the probe state $|\psi'_3\rangle$ in Eqn. 58.

For $0 < \sigma < \frac{\pi}{2}$ and $\cos(\sigma) > 0$, one needs to choose $\mathcal{N}(0) = \cot\left(\frac{\sigma}{2}\right)$, and at the end of the \mathcal{PT} -symmetric evolution, the ζ operator can be found explicitly:

$$\zeta_+^I\left(\tau^I = \frac{\pi}{2\omega}\right) = \frac{1}{2}\sqrt{\cos(\sigma)}\csc\left(\frac{\sigma}{2}\right)\begin{pmatrix} 1 & -i \\ i & 1 \end{pmatrix}, \quad (41)$$

as well as the population of postselected space representing the probability of a conclusive outcome:

$$\mathcal{D}_+^I(m, \sigma) = \frac{1}{2}(1 - \cos(m)\cos(\sigma))\sec^2\left(\frac{\sigma}{2}\right) \quad (42)$$

On the edges corresponding to $|\psi_1\rangle$ and $|\psi_2\rangle$, one finds:

$$\mathcal{D}_+^I(\sigma, \sigma) = \mathcal{D}_+^I(-\sigma, \sigma) = 1 - \cos(\sigma) = 1 - |\cos(\sigma)| \quad (43)$$

For $\frac{\pi}{2} < \sigma < \pi$ and $\cos(\sigma) < 0$, one needs to choose $\mathcal{N}(0) = \tan\left(\frac{\sigma}{2}\right)$ leading to the following ζ operator at the end of evolution:

$$\zeta_-^I\left(\tau^I = \frac{\pi}{2\omega}\right) = \frac{1}{2}\sqrt{-\cos(\sigma)}\sec\left(\frac{\sigma}{2}\right)\begin{pmatrix} 1 & i \\ -i & 1 \end{pmatrix}, \quad (44)$$

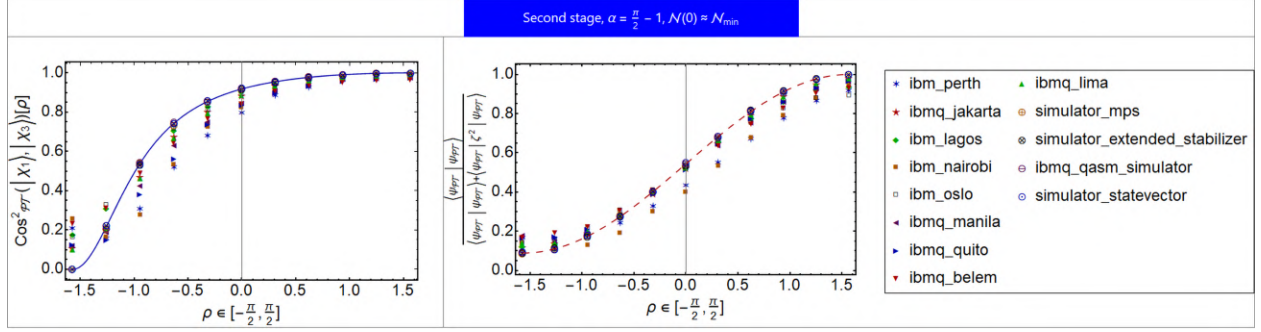


Figure 13. *Stage 2* for $\alpha = \frac{\pi}{2} - 1$.

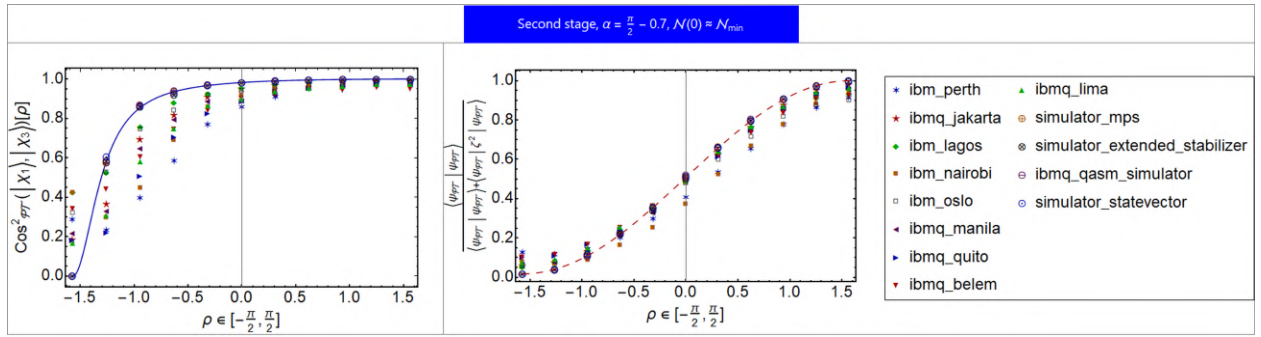


Figure 14. *Stage 2* for $\alpha = \frac{\pi}{2} - 0.7$.

and the corresponding population of postselected space is:

$$\mathcal{D}_-^I(m, \sigma) = \frac{1}{2} (1 - \cos(m) \cos(\sigma)) \csc^2\left(\frac{\sigma}{2}\right), \quad (45)$$

$$\mathcal{D}_-^I(\sigma, \sigma) = \mathcal{D}_-^I(-\sigma, \sigma) = 1 + \cos(\sigma) = 1 - |\cos(\sigma)| \quad (46)$$

Combining Eqns. 43 and 46, one observes that when probability of successful outcome is considered, the \mathcal{PT} -symmetric discrimination of $N = 2$ quantum states developed in [58] converts two reference vectors in Eqn. 6 to orthogonal ones with the probability of the conclusive outcome being $1 - |\cos(\sigma)|$, the same as in a conventional unambiguous quantum state discrimination [13]. We extend this result for $N = 3$ states in the next subsection.

B. Second stage

Similarly, by explicitly computing the ζ operator in this case, we find that the condition on reality of its eigenvalues reduces to:

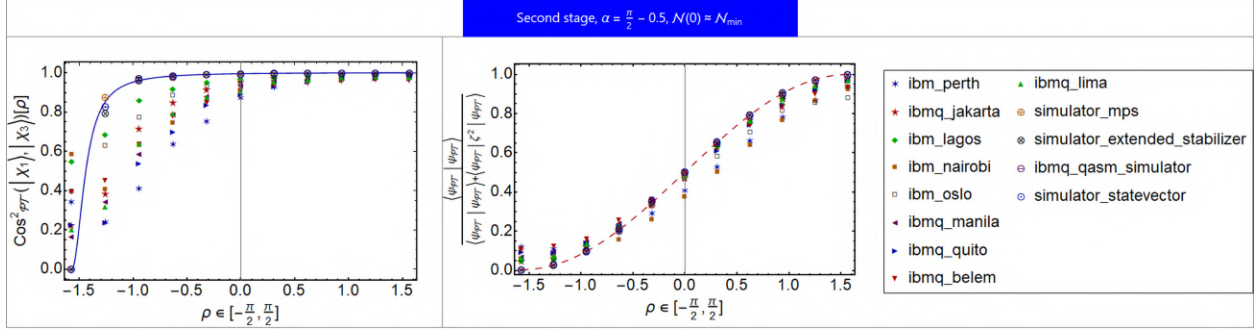


Figure 15. *Stage 2* for $\alpha = \frac{\pi}{2} - 0.5$.

$$\mathcal{N}(0) \geq \frac{1 + \cos(2\alpha)}{2 - \cos(2\omega\tau^{\text{II}}) + \cos(2\alpha) \cos(2\omega\tau^{\text{II}}) \pm 2 \sin(\alpha) \sin(\omega\tau^{\text{II}}) \sqrt{3 + \cos(2\alpha) - 2 \sin^2(\alpha) \cos(2\omega\tau^{\text{II}})}} \quad (47)$$

For $0 \leq \alpha < \frac{\pi}{2}$, one needs to choose the “-” sign which leads to the following ζ operator at the end of evolution:

$$\zeta_+^{\text{II}} \left(\tau^{\text{II}} = \frac{\pi}{2\omega} \right) = \frac{\sqrt{\sin(\alpha)}}{1 - \sin(\alpha)} \begin{pmatrix} 1 & -i \\ i & 1 \end{pmatrix} \quad (48)$$

This leads to the following probability of decisive outcome:

$$\mathcal{D}_+^{\text{II}}(\alpha, \rho) = \frac{3 + 4 \sin(\alpha) \sin(\rho) - \cos(2\alpha)}{3 + 4 \sin(\alpha) - \cos(2\alpha)} \quad (49)$$

Observe that $\mathcal{D}_+^{\text{II}}(\alpha, \rho = \frac{\pi}{2}) = 1$, and in the limit $\alpha \rightarrow \frac{\pi}{2}$:

$$\mathcal{D}_+^{\text{II}}(\alpha, \rho) = \frac{1}{2}(1 + \sin(\rho)) + \frac{1}{32} \left(\frac{\pi}{2} - \alpha \right)^4 (1 - \sin(\rho)) + O \left(\left(\frac{\pi}{2} - \alpha \right)^5 \right) \quad (50)$$

Thus, in this limit, the position $\rho = -\frac{\pi}{2}$ becomes close to almost always inconclusive.

Similarly, for $-\frac{\pi}{2} < \alpha \leq 0$, one chooses the “+” in Eqn. 47 and obtains:

$$\zeta_-^{\text{II}} \left(\tau^{\text{II}} = \frac{\pi}{2\omega} \right) = \frac{\sqrt{-\sin(\alpha)}}{1 + \sin(\alpha)} \begin{pmatrix} 1 & i \\ -i & 1 \end{pmatrix}, \quad (51)$$

$$\mathcal{D}_-^{\text{II}}(\alpha, \rho) = \frac{3 + 4 \sin(\alpha) \sin(\rho) - \cos(2\alpha)}{3 - 4 \sin(\alpha) - \cos(2\alpha)}, \quad (52)$$

and for this case, $\mathcal{D}_-^{\text{II}}(\alpha, \rho = -\frac{\pi}{2}) = 1$, and in the limit $\alpha \rightarrow -\frac{\pi}{2}$:

$$\mathcal{D}_-^{\text{II}}(\alpha, \rho) = \frac{1}{2}(1 - \sin(\rho)) + \frac{1}{32} \left(\alpha + \frac{\pi}{2} \right)^4 (1 + \sin(\rho)) + O \left(\left(\alpha + \frac{\pi}{2} \right)^5 \right) \quad (53)$$

Importantly, combining two cases $\mathcal{D}_\pm^{\text{II}}$, we observe that:

$$\cos_{\mathcal{PT}}^2(\kappa_{23}) \mathcal{D}_+^{\text{II}}(\alpha, \rho) = \frac{(1 - \sin(\alpha))^2(1 - \sin(\rho))}{3 + 4 \sin(\alpha) - \cos(2\alpha)}, \quad (54)$$

$$\cos_{\mathcal{PT}}^2(\kappa_{13}) \mathcal{D}_-^{\text{II}}(\alpha, \rho) = \frac{(1 + \sin(\alpha))^2(1 + \sin(\rho))}{3 - 4 \sin(\alpha) - \cos(2\alpha)} \quad (55)$$

And similarly:

$$\cos_{\mathcal{PT}}^2(\kappa_{13}) \mathcal{D}_+^{\text{II}}(\alpha, \rho) = \frac{1 + \sin(\rho)}{2} = \cos^2 \left(\frac{\frac{\pi}{2} - \rho}{2} \right), \quad (56)$$

$$\cos_{\mathcal{PT}}^2(\kappa_{23}) \mathcal{D}_-^{\text{II}}(\alpha, \rho) = \frac{1 - \sin(\rho)}{2} = \cos^2 \left(\frac{\frac{\pi}{2} + \rho}{2} \right) \quad (57)$$

From Eqns. 54 and 55, one can observe that when the probability of the decisive outcome is taken into account, the \mathcal{PT} -symmetric transformation on the second stage does not improve the state distinguishability. The state in the \mathcal{PT} -symmetric exceptional point ($|\chi_1\rangle$ or $|\chi_2\rangle$) has a low probability of the conclusive outcome. The state $|\chi_3\rangle$ has a small projection on the reference vector corresponding to the exceptional point, but its decisiveness is much higher, as one can observe in Eqns. 49 and 52, in such a way that average error rate remains the same since all values of ρ in Eqns. 54 and 55 are rescaled by the same factor. Similarly, from Eqns. 56 and 57, one observes that an increase in $\cos_{\mathcal{PT}}^2$ is accompanied by reduction of $\mathcal{D}_\pm^{\text{II}}$ and thus on *average* one obtains the same result as in the Hermitian case.

However, as we discuss in Section VIII, the capability to consolidate all relevant information regarding the parameter of interest within a small subset of events can be inherently advantageous. Furthermore, when utilizing a non-MSE performance metric—such as, for instance, $\cos_{\mathcal{PT}}^4 \times \mathcal{D}_\pm^{\text{II}}$ instead of $\cos_{\mathcal{PT}}^2 \times \mathcal{D}_\pm^{\text{II}}$ —it becomes evident that \mathcal{PT} -symmetric sensing can offer advantages over its Hermitian counterpart.

In the next Section VI, we confirm our analytical results by numerical computations and simulation on IBM Quantum Experience.

VI. IMPLEMENTATION AND EXPERIMENTAL RESULTS

IBM Quantum Experience [67] is a quantum processor operating on superconducting qubits that has become a leading candidate for scalable quantum computing platform, see

a review [68]. These devices already enabled proof-of-concept results such as quantum error correction [69], fault-tolerant gates [70], experimental evidence of the violation of Mermin and Leggett-Garg inequalities [71, 72], non-local parity measurements [73, 74], simulations of paradigmatic models in open quantum systems [75], creation of highly entangled graph states [76], determining the ground-state energies of the molecules [77] as well as implementation of quantum witnesses [78]. Moreover, \mathcal{PT} -symmetric quantum mechanics can enhance entanglement by local operations, a possibility prohibited in the Hermitian case, as demonstrated experimentally by IBM Quantum Experience [62] based on theoretical findings from [79].

We implement *Stage 1* of our algorithm for $\sigma = \frac{4}{5}$ and $\frac{6}{5}$. To illustrate the changes in the geometry of the postselected space, we examine the third state in two forms, $|\psi_3\rangle$ and $|\psi'_3\rangle$:

$$|\psi_3\rangle = \begin{pmatrix} \cos\left(\frac{\pi+2\delta}{4}\right) \\ -i \sin\left(\frac{\pi+2\delta}{4}\right) \end{pmatrix}, |\psi'_3\rangle = \begin{pmatrix} \cos\left(\frac{\pi+2\Delta}{4}\right) \\ e^{i\varphi} \sin\left(\frac{\pi+2\Delta}{4}\right) \end{pmatrix} \quad (58)$$

In Figs. 4 and 5, theoretical predictions from Section V are shown. One can observe that a higher value of σ corresponds to the higher value of the population of the postselected subspace and steeper curves. Fig. 6 corresponds to the *Stage 2* as α parameter approaches the exceptional point $\frac{\pi}{2}$, and one can observe that as the value of $\cos^2_{\mathcal{PT}}$ flattens out, the probability of a decisive outcome at $\rho = -\frac{\pi}{2}$ approaches zero.

We implemented both *Stage 1* and *2* on IBM Quantum Experience with the details provided in Methods. We performed experiments on all processors provided by IBM Quantum Experience, namely `ibm_perth`, `ibmq_jakarta`, `ibm_lagos`, `ibm_nairobi`, `ibm_oslo`, `ibmq_manila`, `ibmq_quito`, `ibmq_belem`, `ibmq_lima`, `simulator_mps`, `simulator_extended_stabilizer`, `ibmq_qasm_simulator`, `simulator_statevector`. In each experiment, total number of shots was kept $N_{shots} = 8192$, and $N(|ij\rangle)$, $i \in [0, 1]$ is a number of outcomes corresponding to $|ij\rangle$, such that $\sum_{i,j=1,2} N(|ij\rangle) = N_{shots}$.

For both *Stages*, the cosine squared between the reference vectors in \mathcal{PT} -symmetric subspace is measured by the postselection as shown in Eqn. 59:

$$\cos^2_{\mathcal{PT}}(|\chi_1\rangle, |\chi_3\rangle) = \frac{N(|00\rangle)}{N(|00\rangle) + N(|10\rangle)}, \quad (59)$$

while the population of the \mathcal{PT} -symmetric subsystem is shown in Eqn. 60, correspondingly:

$$\mathcal{D} = \frac{\langle \psi_{\mathcal{PT}} | \psi_{\mathcal{PT}} \rangle}{\langle \psi_{\mathcal{PT}} | \psi_{\mathcal{PT}} \rangle + \langle \psi_{\mathcal{PT}} | \zeta^2 | \psi_{\mathcal{PT}} \rangle} = \frac{N(|00\rangle) + N(|10\rangle)}{N(|00\rangle) + N(|10\rangle) + N(|01\rangle) + N(|11\rangle)} \quad (60)$$

For *Stage 1*, the comparison between theoretical predictions and experimental results are shown in Figs. 7, 8, 9, 10, 11, and 12. For *Stage 2*, the corresponding comparison is

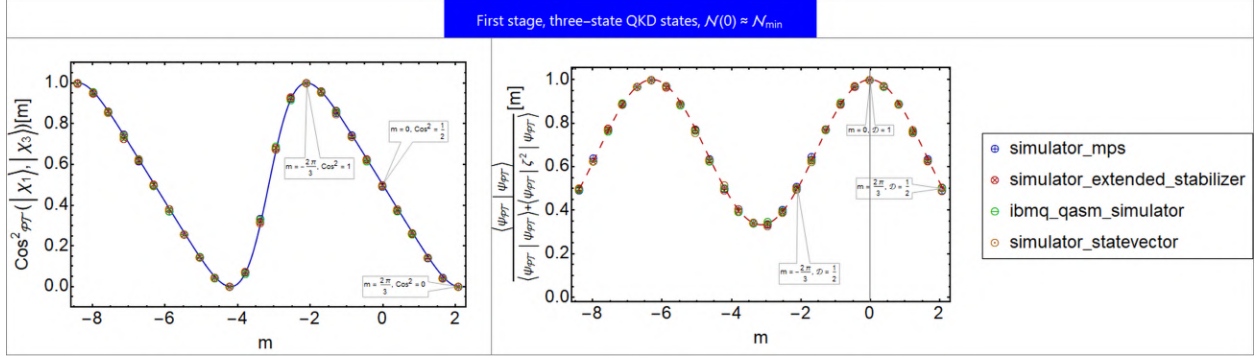


Figure 16. *Stage 1* for the states in Eqn. 37 with $\sigma = \frac{2\pi}{3}$ and $\mathcal{N}(0) \approx \mathcal{N}_{min}$. The state corresponding to $m = 0$ always yields a conclusive result $\mathcal{D} = 1$.

provided in Figs. 13, 14, and 15. In both *Stages*, it is evident that the simulator_mps, simulator_extended_stabilizer, ibmq_qasm_simulator, and simulator_statevector provided by IBM processors, as indicated by circles, consistently exhibit superior agreement with theoretical predictions. Other processors, while successfully capturing the overall shapes of the theoretical curves, have significant deviations. This may imply that quantum processors employing a Matrix Product State representation, ranked-stabilizer decomposition, Open Quantum Assembly Language, and those characterizing the quantum state of a system through a state vector are particularly well-suited for performing \mathcal{PT} -symmetric algorithms on IBM Quantum Experience [67].

Thus, we used these four simulators, namely simulator_mps, simulator_extended_stabilizer, ibmq_qasm_simulator, and simulator_statevector, to perform simulation of attack three-state QKD protocol [80]. The states used in this QKD protocol have $\frac{2\pi}{3}$ angular separation:

$$|A\rangle = \begin{pmatrix} 1 \\ 0 \end{pmatrix}, |B\rangle = \begin{pmatrix} \frac{1}{2} \\ -\frac{\sqrt{3}}{2} \end{pmatrix}, |C\rangle = \begin{pmatrix} -\frac{1}{2} \\ -\frac{\sqrt{3}}{2} \end{pmatrix} \quad (61)$$

The following operation:

$$K = \begin{pmatrix} \frac{1}{\sqrt{2}} & \frac{i}{\sqrt{2}} \\ \frac{1}{\sqrt{2}} & -\frac{i}{\sqrt{2}} \end{pmatrix}, \quad (62)$$

converts the reference states in Eqn. 61 our conventions in Eqn. 37 as: $|\psi_m, m = 0\rangle \rightarrow |A\rangle$, $|\psi_m, m = \frac{2\pi}{3}\rangle \rightarrow |B\rangle$, $|\psi_m, m = -\frac{2\pi}{3}\rangle \rightarrow |C\rangle$. Since $\cos(\frac{2\pi}{3}) < 0$, we use Eqn. 45 for the probability of decisive outcome.

In Fig. 16, one can observe a remarkable agreement between theoretical predictions for *Stage 1* from Section V and experimental results from simulator_mps, simulator_extended_stabilizer,

ibmq_qasm_simulator, and simulator_statevector. For the specific geometry of states described in Eqn.61, it can be observed that *Stage 1*, with the value of α determined by Eqn.36 and $\mathcal{N}(0) = \mathcal{N}_{min}$, transforms these states into a mirror-symmetric configuration. In this configuration, $|B\rangle$ and $|C\rangle$ become orthogonal to each other, with $|A\rangle$ positioned between them. Regarding the probability of a decisive outcome, one can observe in Fig. 16 that: $\mathcal{D}(|B\rangle) = \mathcal{D}(|C\rangle) = \frac{1}{2}$ while $\mathcal{D}(|A\rangle) = 1$. Thus, the states $|B\rangle$ and $|C\rangle$ are 50% conclusive while the state $|A\rangle$ is always conclusive. In the upcoming Section VII, we delve into the implications of these observations and conduct a comparative analysis of our protocol against existing approaches for attacking this QKD protocol.

VII. ATTACK ON THE TRINE-STATE QKD PROTOCOL

The available strategies for the attack on three-state QKD protocol are minimum error and maximum mutual information approaches [80]. For the geometry of states in Eqn. 61, minimum error and maximum confidence strategies coincide [3], and thus we do not consider the latter.

If the encoded state is $|A\rangle$, minimum error discrimination strategy yields correct result with the probability $\frac{2}{3}$, and misclassifies $|A\rangle$ as being $|B\rangle$ or $|C\rangle$ with the probability $\frac{1}{6}$. The same applies for $|B\rangle$ and $|C\rangle$ through the permutation $A \rightarrow B \rightarrow C$. For minimum error strategy obtaining $|A\rangle$ after the measurement, the resulting density matrix is [80]:

$$\rho_{Min.err.} = \frac{2}{3} |A\rangle \langle A| + \frac{1}{6} |B\rangle \langle B| + \frac{1}{6} |C\rangle \langle C| \quad (63)$$

The maximum mutual information strategy excludes one of the states with certainty, but the other two states remain equiprobable each with 50% probability and the resulting density matrix:

$$\rho_{Max.mut.inf.} = \frac{1}{2} |\bar{B}\rangle \langle \bar{B}| + \frac{1}{2} |\bar{C}\rangle \langle \bar{C}|, \quad (64)$$

where $|\bar{B}\rangle$ and $|\bar{C}\rangle$ are complementary to $|B\rangle$ and $|C\rangle$ [80]. However, both of these strategies yield the same error rate, as demonstrated by [80], attributed to the inherent geometric properties of these states since:

$$\rho_{Min.err.} = \rho_{Max.mut.inf.} = \frac{1}{2} |A\rangle \langle A| + \frac{1}{4} \quad (65)$$

Now, consider the case when the attacker uses our \mathcal{PT} -symmetric approach for $N = 3$ states we developed in the previous Sections. If *Stage 1*, as described in the preceding Section VI, produces an inconclusive result, the attacker immediately eliminates one of the

states with 100% confidence. This is because the probability of obtaining a decisive outcome for one state is 100%, while the other two states are equiprobable, as illustrated in Fig. 16. For a particular choice in Fig. 16, the attacker eliminates the state $|A\rangle$ leaving $|B\rangle$ and $|C\rangle$ equiprobable. The probability of an inconclusive result in *Stage 1* is given by:

$$p\left(|1\rangle_{ancilla}^I\right) = \frac{1}{3} \cdot \frac{1}{2} + \frac{1}{3} \cdot 0 + \frac{1}{3} \cdot \frac{1}{2} = \frac{1}{3} \quad (66)$$

Thus, with probability $\frac{1}{3}$, our approach yields the result equivalent to the maximum mutual information strategy.

In case the first postselection is successful, which happens with $\frac{2}{3}$ probability, the resulting postselected geometry of the states is mirror-symmetric. However, since the postselection probability is nonuniform and varies for different states, their prior probabilities used as input for the next *Stage* change from equiprobable to the values:

$$p\left(|A\rangle, |0\rangle_{ancilla}^I\right) = \frac{1 \cdot \frac{1}{3}}{\frac{2}{3}} = \frac{1}{2}, p\left(|B\rangle, |0\rangle_{ancilla}^I\right) = p\left(|C\rangle, |0\rangle_{ancilla}^I\right) = \frac{\frac{1}{2} \cdot \frac{1}{3}}{\frac{2}{3}} = \frac{1}{4} \quad (67)$$

At this point, the attacker may choose to apply the strategy for mirror-symmetric configuration [16] with $p = \frac{1}{4}$. In this scenario, the success probability rate remains $\frac{2}{3}$, consistent with the original attack outlined in [80], as indicated by Eqn.(14) in [16]. Despite the change in the geometry of the postselected space, the success rate remains unchanged due to the varying probabilities of successful postselections for the states in Eqn. 61.

Alternatively, if the attacker proceeds with *Stage 2*, as discussed in Section V, one of the states— $|B\rangle$ or $|C\rangle$ —will have a 100% probability of successful postselection, depending on whether α is greater or less than zero. Thus, if postselection of the *Stage 2* fails, the attacker immediately eliminates one of these states. For definiteness, let $\alpha > 0$ and consider the probability of a decisive outcome as given in Eqn. 49. In this case, one finds:

$$1 - \mathcal{D}_+^{\text{II}}\left(\alpha, \rho = -\frac{\pi}{2}\right) = 2\left(1 - \mathcal{D}_+^{\text{II}}(\alpha, \rho = 0)\right) = \frac{4 \sin(\alpha)}{(1 + \sin(\alpha))^2} \quad (68)$$

Considering Eqns. 67 and 68, it is observed that the states $|A\rangle$ and $|C\rangle$ become equiprobable while the state $|B\rangle$ is eliminated:

$$p\left(|A\rangle, |1\rangle_{ancilla}^{\text{II}}\right) p\left(|A\rangle, |0\rangle_{ancilla}^I\right) = p\left(|C\rangle, |1\rangle_{ancilla}^{\text{II}}\right) p\left(|C\rangle, |0\rangle_{ancilla}^I\right) \quad (69)$$

As a result, the scenario in which the second postselection fails, $|1\rangle_{ancilla}^{\text{II}}$, is equivalent to a maximum mutual information strategy.

If the postselection for *Stage 2* is successful but the measurement returns the value corresponding to the projection on $\rho = \frac{\pi}{2}$, the attacker eliminates the state $|C\rangle$ corresponding

to $\rho = -\frac{\pi}{2}$ since in this case $\cos_{\mathcal{PT}}^2(\rho = -\frac{\pi}{2}) = 0$, as illustrated in Fig. 6. Similarly, the remaining two states, $|A\rangle$ and $|B\rangle$, remain equiprobable since:

$$p\left(|B\rangle, |0\rangle_{\text{ancilla}}^{\text{I}}\right) \cos_{\mathcal{PT}}^2\left(\kappa_{13}, \rho = \frac{\pi}{2}\right) \mathcal{D}_+^{\text{II}}\left(\alpha, \rho = \frac{\pi}{2}\right) = \frac{1}{4}, \quad (70)$$

$$p\left(|A\rangle, |0\rangle_{\text{ancilla}}^{\text{I}}\right) \cos_{\mathcal{PT}}^2(\kappa_{13}, \rho = 0) \mathcal{D}_+^{\text{II}}(\alpha, \rho = 0) = \frac{1}{4} \quad (71)$$

Finally, if the postselection at the *Stage 2* is successful, and the measurement yields the state with $\rho = -\frac{\pi}{2}$ projection corresponding to $|C\rangle$, the state $|B\rangle$ is excluded. Similarly, one observes that:

$$p\left(|C\rangle, |0\rangle_{\text{ancilla}}^{\text{I}}\right) \mathcal{D}_+^{\text{II}}\left(\alpha, \rho = -\frac{\pi}{2}\right) = p\left(|A\rangle, |0\rangle_{\text{ancilla}}^{\text{I}}\right) \mathcal{D}_+^{\text{II}}(\alpha, \rho = 0) \cos_{\mathcal{PT}}^2(\kappa_{23}, \rho = 0), \quad (72)$$

and thus the states $|A\rangle$ and $|C\rangle$ remain equiprobable.

In summary, coupling *Stage 1* of our algorithm with a strategy for discriminating mirror-symmetric states, as developed in [16], results in an outcome equivalent to the maximum mutual information strategy in $\frac{1}{3}$ of the cases and, in $\frac{2}{3}$ of the cases, yields the same result as the minimum-error strategy. If both *Stages* are employed, our approach yields an equivalent result to the maximum mutual information strategy. Given that the minimum error and maximum mutual information strategies exhibit the same error rate for this QKD protocol due to Eqn. 65, our algorithm achieves precisely the same error rate as these strategies in both cases. However, in the next Section VIII, we pinpoint applications where our algorithm is advantageous to its Hermitian counterparts.

VIII. DISCUSSION AND APPLICATIONS

While our algorithm does not provide an advantage for the specific states used in the three-states QKD protocol, as given in Eqn. 61, it can be advantageous in other scenarios. In cases involving highly nonsymmetric states, where explicit solutions are not readily available and intricate computations are required [18], our approach's ability to map three arbitrary states to a predefined and standardized set can be beneficial in practical applications.

As discussed in Section IV, our algorithm enables the mapping of three *arbitrary* states to stabilizer states, albeit with the adjustment of their prior probabilities. Stabilizer states play a pivotal role in quantum error correction, serving as the operational foundation for numerous quantum error correction codes [65, 81]. They enable the detection and correction of errors in quantum systems, thereby proving essential for the development of reliable and fault-tolerant quantum computers [65, 81]. This capability holds significant implications for quantum error

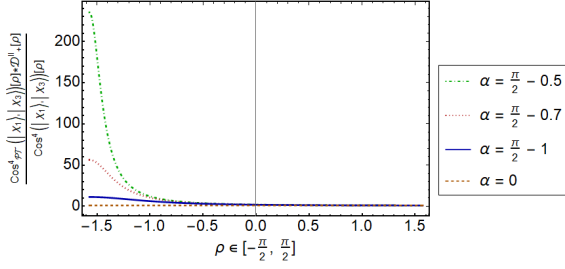


Figure 17. Comparison of $\cos^4_{\mathcal{PT}}$ in \mathcal{PT} -symmetric subsystem weighted by the population of postselected space to its Hermitian counterpart.

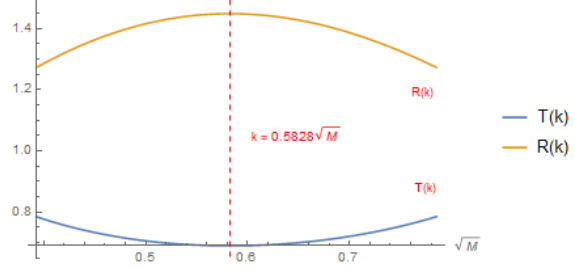


Figure 18. Minimization of the average number of oracle calls and maximization of probability over the average number of oracle calls corresponding to $T(k)$ and $R(k)$.

correction, particularly considering the absence of a single, universally applicable quantum error correction code for an arbitrary set of states [82]. The ability to map *arbitrary* three states onto stabilizer states while conserving their projections on reference vectors has the potential to enhance error protection, encompassing a broader spectrum of errors and thereby contributing to the advancement of quantum memory capabilities.

With the explicit expressions for the probability of the decisive outcome of \mathcal{PT} -symmetric evolution derived in Section V, we can now assess its implications for quantum sensing applications. It has been demonstrated that probabilistic metrology, evaluated based on the mean-square estimation error (MSE), fails to enhance the quantum limits of single-parameter estimation [83]. Remarkably, it has been highlighted that this conclusion *might not hold true* when alternative non-MSE performance metrics are used [83]. Furthermore, the usage of non-Hermitian single-qubit gates for quantum sensing was proposed [84] since such systems exhibit divergent susceptibility promising an enhanced sensitivity. At the same time, it was recently shown that when the postselection probability is taken into account, the *average* QFI does not increase [85].

Our results align with the findings of all the aforementioned works. Namely, in Fig. 6, one can observe a sharp spike in sensitivity at $\rho = -\frac{\pi}{2}$ in terms of $\cos^2_{\mathcal{PT}}$ reminiscent of [84]. At the same time, similarly to [37, 38], for the density matrix ρ_{init} corresponding to the pure state $|\chi_3\rangle$ in Eqn. 15, we compute QFI \mathcal{F}_ρ^{Pure} after the *Stage 2* of \mathcal{PT} -symmetric evolution:

$$\rho^{Stage\ 2}(t) = \frac{e^{-i\mathcal{H}t} \rho_{init} e^{i\mathcal{H}^\dagger t}}{\text{Tr}(e^{-i\mathcal{H}t} \rho_{init} e^{i\mathcal{H}^\dagger t})}, \quad \mathcal{F}_\rho^{Pure} = 2\text{Tr} \left[\left(\partial_\rho \rho^{Stage\ 2} \left(t = \tau^{\text{II}} = \frac{\pi}{2\omega} \right) \right)^2 \right] \quad (73)$$

One observes at $\rho = -\frac{\pi}{2}$ an apparently divergent QFI, similarly to [84]:

$$\mathcal{F}^{\mathcal{PT}}(\alpha, \rho) = \frac{4 \cos^4(\alpha)}{(3 + 4 \sin(\alpha) \sin(\rho) - \cos(2\alpha))^2} = \frac{(\alpha - \frac{\pi}{2})^4}{4(1 + \sin(\rho))^2} + O\left(\left(\alpha - \frac{\pi}{2}\right)^5\right), \quad (74)$$

However, by an explicit computation, one obtains:

$$\mathcal{F}^{\mathcal{PT}}\left(\alpha, \rho = -\frac{\pi}{2}\right) \mathcal{D}_+^{\text{II}}\left(\alpha, \rho = -\frac{\pi}{2}\right) = 1 \quad (75)$$

Thus, an *average* QFI remains the same as in the Hermitian case, in complete agreement with [85].

These results have several implications for practical applications. First, as discussed in [86], even though an average QFI after the postselection remains the same as in the Hermitian case, the ability to “condense” all QFI about the detected parameter into a small fraction of events by itself gives technical advantages. Also, given that the value of $\cos_{\mathcal{PT}}^2$ in the postselected space is larger than its Hermitian counterpart, this property can be useful for realistic detectors with the sensitivity threshold.

Secondly, when non-MSE performance metrics are utilized, \mathcal{PT} -symmetric metrology can be notably superior to the Hermitian counterpart. For instance, replacing $\cos_{\mathcal{PT}}^2(|\chi_1\rangle, |\chi_3\rangle) \times \mathcal{D}_+^{\text{II}}$ by $\cos_{\mathcal{PT}}^4(|\chi_1\rangle, |\chi_3\rangle) \times \mathcal{D}_+^{\text{II}}$ illustrates this potential advantage. The ratio of the fourth power of the cosine in postselected space, weighted by the probability of the decisive outcome $\cos_{\mathcal{PT}}^4(|\chi_1\rangle, |\chi_3\rangle) \times \mathcal{D}_+^{\text{II}}$, to the fourth power of the corresponding cosine in Hermitian space is depicted in Fig. 17. One can observe a notable peak in Fig. 17 at $\rho = -\frac{\pi}{2}$ when $\alpha \rightarrow \frac{\pi}{2}$, since using Eqn. 56:

$$\frac{\cos_{\mathcal{PT}}^4(|\chi_1\rangle, |\chi_3\rangle) \times \mathcal{D}_+^{\text{II}}}{\cos^4(|\chi_1\rangle, |\chi_3\rangle)} = \frac{\cos_{\mathcal{PT}}^2(|\chi_1\rangle, |\chi_3\rangle)}{\cos^2(|\chi_1\rangle, |\chi_3\rangle)} \quad (76)$$

This result is consistent with [83], where it was emphasized that for non-MSE loss functions, \mathcal{PT} -symmetric metrology can be superior to the Hermitian one. This property can be useful in quantum sensing which involves dealing with noisy data. Given the sensitivity of MSE to outliers and its tendency to overestimate noisy data points, using a non-MSE loss function that penalizes deviations from the true value more strongly than a quadratic loss function can improve robustness to outliers and improve overall performance.

Our methodology has the potential to be advantageous in the parallelization of quantum computations, aiming to decrease circuit depth. The depth parameter is crucial for Noisy Intermediate Scale Quantum (NISQ) computers defined by Preskill [87]. These quantum computers feature noisy qubits and have the potential to solve practical problems of commercial significance faster than conventional supercomputers or with lower energy consumption. To address the challenges posed by error accumulation, decoherence, and error

correction, it is recommended that the corresponding quantum circuits exhibit a shallow depth corresponding to a small number of qubit gate cycles [88]. Additionally, the NIST call for proposals on Post-Quantum Cryptography (PQC) [89, 90] emphasized a specific form of the quantum circuit model. In this variant, the adversary is constrained to executing a maximum of MAXDEPTH gates in series.

Our algorithm may find application in the parallelization of quantum phase estimation, a critical component of Shor’s algorithm [91, 92]. To illustrate, consider the case of a single qubit, represented as $|\psi_\Phi\rangle = \frac{1}{\sqrt{2}} (|0\rangle + e^{2\pi i\Phi} |1\rangle)$, where Φ denotes the phase to be estimated. For a single qubit, the inverse Quantum Fourier Transform (QFT) is represented by the Hadamard gate. This operation alters the state of the qubit to:

$$|\psi_\Phi\rangle \rightarrow \begin{pmatrix} \cos(\pi\Phi) \\ -i \sin(\pi\Phi) \end{pmatrix}, \quad (77)$$

To enhance the measurement accuracy of a small value of Φ , one can apply the unitary operator of interest multiple times *in series* before performing the measurement. However, it is important to note that in this approach, the depth of the quantum circuit would become substantial, rendering it more susceptible to the accumulation of errors. An alternative strategy that we propose involves applying *Stage 2*, as described in Section V. This effectively increases the value of Φ at the expense of reducing the probability of a decisive outcome. Eqn. 56 shows that, on average, the increase in the phase needed to be estimated will be the same in both cases. However, by employing *Stage 2* of \mathcal{PT} -symmetric evolution from Section V, this increase will be executed *in parallel*. This parallel implementation holds significant potential for reducing susceptibility to errors.

Finally, consider our approach in application for the search over an unstructured database of size $M = 2^n$. The renowned Grover’s search algorithm [93] finds the solution in time $\sim \sqrt{M}$ and is optimal in terms of the number of oracle calls required for the search process [94]. The possibility to improve the search over an unstructured database by using \mathcal{PT} symmetry was introduced in [58] (referring to [11]) and further discussed in [95]. In the conventions of [11], following the application of the oracle *only once*, the state of the last qubit is:

$$\frac{2^n}{\sqrt{2^{2n} - 2^{n+1}s + 2s^2}} \left(\frac{2^n - s}{2^n} |0\rangle + \frac{s}{2^n} |1\rangle \right), \quad (78)$$

where s represents the number of solutions. For simplicity, we consider the case of $s = 1$ solution further in the text. According to [11], the ability to exponentially separate the states $|0\rangle$ and $|1\rangle$ implies the capability to search exponentially large databases in polynomial time. However, as discussed in [95], achieving such an operation is only possible with an exponentially small probability of success. Consequently, it is not feasible to search over an

unstructured database using a fewer number of oracle calls than in Grover's algorithm. Our results in Eqns. 56 and 57 are in complete agreement with [95]. After applying the following unitary transformation:

$$Q = \begin{pmatrix} \frac{1}{\sqrt{2}} & \frac{1}{\sqrt{2}} \\ -\frac{i}{\sqrt{2}} & \frac{i}{\sqrt{2}} \end{pmatrix}, \quad (79)$$

and using *Stage 2*, it is possible to exponentially increase the value of $\cos^2_{\mathcal{PT}}$ as shown in Section V. However, this enhancement is counterbalanced by an exponential decrease in postselection probability \mathcal{D}^{II} , resulting in no improvement in the average number of oracle calls.

However, Grover's search algorithm was shown to be *not* depth-optimal [96]. Thus, instead of attempting the impossible task of reducing the number of oracle calls [94], our proposal involves leveraging our \mathcal{PT} -symmetric algorithm to optimize the *depth* of the quantum circuit required for a quantum database search, as demonstrated further in the text.

As the quantum state of Grover's algorithm remains in a two-dimensional subspace after each application of the oracle [93], our results developed for the qubit case in Section V are directly applicable to the unstructured database search as well. Let $|\omega\rangle$ be the state to be identified, $|s\rangle = \frac{1}{\sqrt{M}} \sum_{x=0}^{M-1} |x\rangle$ the initial state before applying the oracles, and $|s'\rangle = \frac{1}{\sqrt{M-1}} \sum_{x \neq \omega} |x\rangle$ the state orthogonal to $|\omega\rangle$. In the limit $M \gg 1$, the state of the system after applying the oracle k times, in the two-dimensional basis formed by orthogonal states $|s'\rangle$ and $|\omega\rangle$, is given by [93]:

$$|\Psi_G\rangle = \begin{pmatrix} \cos\left(\frac{2k}{\sqrt{M}}\right) \\ \sin\left(\frac{2k}{\sqrt{M}}\right) \end{pmatrix}, \quad (80)$$

After applying the oracle $k_f = \frac{\pi}{4}\sqrt{M}$ times, the probability of correctly identifying the state

$$p_+(k) = \sin^2\left(\frac{2k}{\sqrt{M}}\right), \quad (81)$$

approaches 100% [93].

The parallelized version of Grover's algorithm [97] provides a decrease in the *average* number of oracle calls by minimizing:

$$T(k) = \sum_{i=1}^{\infty} (1 - p_+(k))^{i-1} p_+(k) ik = k \csc^2\left(\frac{2k}{\sqrt{M}}\right) \rightarrow \min \quad (82)$$

This improvement capitalizes on the observation that the convergence towards the end of the complete Grover's search algorithm is slow, as indicated in Eqn. 80. The search is stopped

after approximately $0.5828\sqrt{M}$ oracle applications, earlier than in the original version of Grover's algorithm ($\frac{\pi\sqrt{M}}{4}$). While the probability of correctly identifying the state is approximately 84.458%, with the risk of having to restart the search, the *average* number of oracle calls is reduced by 12% [97].

Our objective is to decrease the *depth* of the circuit while maintaining the same average number of oracle calls. This will be achieved through the application of the \mathcal{PT} -symmetric transformation, as elaborated in Section V. After an initial application of the oracle k_{Init} times, the Q transformation in Eqn. 79 on the two-dimensional subspace of Eqn. 80 converts $|\Psi_G\rangle$ to:

$$|\Psi_G\rangle \rightarrow \begin{pmatrix} \cos\left(\frac{2k_{Init}}{\sqrt{M}} - \frac{\pi}{4}\right) \\ -i \sin\left(\frac{2k_{Init}}{\sqrt{M}} - \frac{\pi}{4}\right) \end{pmatrix} \quad (83)$$

One can use *Stage 2* outlined in Section V, guided by Eqn.56, along with the inverse of Q as defined in Eqn.79. This enhances the projection of $|\Psi_G\rangle$ onto $|\omega\rangle$ but comes at the expense of diminishing the likelihood of a conclusive outcome.

Before application of the \mathcal{PT} -symmetric evolution:

$$p_+(k_{Init}) = \sin^2\left(\frac{2k_{Init}}{\sqrt{M}} - \frac{\pi}{4}\right), \quad \mathcal{D}_+^{\text{II}}(k_{Init}) = 1 \quad (84)$$

After the application of *Stage 2*, one observes an effective value k_{Eff} exceeding the initial value k_{Init} , as depicted in Fig. 6. However, in accordance with Eqn.56, the following quantity remains constant:

$$p_+(k_{Eff}) \mathcal{D}_+^{\text{II}}(k_{Eff}) = \sin^2\left(\frac{2k_{Init}}{\sqrt{M}} - \frac{\pi}{4}\right) \cdot 1, \quad (85)$$

and as a result of *Stage 2*:

$$p_+(k_{Eff}) = \sin^2\left(\frac{2k_{Eff}}{\sqrt{M}} - \frac{\pi}{4}\right), \quad \mathcal{D}_+^{\text{II}}(k_{Eff}) = \frac{\sin^2\left(\frac{2k_{Init}}{\sqrt{M}} - \frac{\pi}{4}\right)}{\sin^2\left(\frac{2k_{Eff}}{\sqrt{M}} - \frac{\pi}{4}\right)} \quad (86)$$

By analogy to minimizing the average number of oracle calls, as expressed in Eqn. 82 in the conventional parallelized Grover's search algorithm [97], the maximization of probability of successful database search while minimizing the average number of oracle calls through the utilization of \mathcal{PT} -symmetric transformation:

$$R(k_{Eff}) = \sum_{i=1}^{\infty} \frac{(1 - \mathcal{D}_+^{\text{II}}(k_{Eff}))^{i-1} \mathcal{D}_+^{\text{II}}(k_{Eff}) p_+(k_{Eff})}{k_{Eff}} = \frac{\sin^2\left(\frac{2k_{Eff}}{\sqrt{M}}\right)}{k_{Eff}} \rightarrow \max, \quad (87)$$

leads to the same optimal value of oracle calls $k_{Opt} = 0.5828\sqrt{M}$ as shown in Fig. 18. According to Eqn. 56, the average number of oracle calls remains unchanged from the original parallelized version of Grover’s algorithm. Nonetheless, it allows the application of oracles in *parallel* rather than in series. As a result, the initial circuit depth of $k_{Opt} = 0.5828\sqrt{N}$ can be significantly reduced to k_{Init} as α approaches $\frac{\pi}{2}$, resulting in $k_{Init} \ll k_{Opt}$. This has promising implications for improving the fault tolerance of Grover’s algorithm, in particular for mitigating the effects of a faulty oracle [98]. In practical scenarios, as depicted in Figs. 13, 14, and 15, the aforementioned advantage may be constrained by the noise effects inherent in real-life quantum processors, particularly as α approaches $\frac{\pi}{2}$.

IX. CONCLUSIONS AND FUTURE WORK

We developed a new \mathcal{PT} -symmetric algorithm for mapping three arbitrary quantum states and verified it using IBM Quantum Experience. Our framework is very flexible and general, accommodating several important partial cases. By deriving exact expressions for the probability of successful postselection, we demonstrated consistency with the Hermitian cases considered in the literature. We demonstrated that in a partial case of $N = 2$ states, our approach provides an equivalent result to the conventional unambiguous quantum state discrimination. When applied for the attack on the three-state QKD protocol, our approach gives the same error rate as other approaches available in the literature and thus is consistent with the security proof of this QKD protocol. By explicit computation, we show the invariance of QFI by the \mathcal{PT} -symmetric operation, in agreement with other results available in the literature. However, we identify the scenarios where our proposed scheme has the potential to outperform its Hermitian counterparts. First, we show when non-MSE performance metrics is used, our scheme is advantageous. Second, when applied for quantum database search, while our scheme uses the same number of oracle calls, it provides a notable reduction of the circuit depth in comparison to the conventional parallelized Grover’s search algorithm. We argue that in the same way quantum phase estimation, which is an important part of Shor’s algorithm, can be parallelized using our proposed algorithm. Additionally, our methodology can be beneficial in practical scenarios for quantum error correction and quantum state discrimination of highly asymmetric states. With our approach already implemented as an optical scheme [60], our work lays the foundation for leveraging the unique properties of \mathcal{PT} symmetry to advance quantum information processing, communication, cryptography, and sensing.

ACKNOWLEDGEMENTS

This publication is based on work supported by a grant from the U.S. Civilian Research & Development Foundation (CRDF Global), award number G-202105-67836. YB was funded in part by the UCCS BioFrontiers Center and the UCCS Cyber Seed Grant. The authors express their gratitude for valuable discussions with Manohar Raavi and Anatoliy Pinchuk during the initial stages of this work.

DATA AND CODE AVAILABILITY

The code, implementation, and results of the runs on the IBM Quantum Experience are publicly available at GitHub repository:

<https://github.com/BalytskyiJaroslaw/QuantumSimulations/tree/master>.

METHODS

Adjusting to convenient positions

A set of arbitrary three states $|\psi_i\rangle = \begin{pmatrix} \cos(\frac{\theta_i}{2}) \\ e^{i\phi_i} \sin(\frac{\theta_i}{2}) \end{pmatrix}$, $i \in [1, 3]$ can be adjusted to the starting positions in Eqn. 9 by the following unitary rotation:

$$\mathcal{R} = \begin{pmatrix} \cos(\frac{\pi-2\sigma}{4}) & -i \sin(\frac{\pi-2\sigma}{4}) \\ -i \sin(\frac{\pi-2\sigma}{4}) & \cos(\frac{\pi-2\sigma}{4}) \end{pmatrix} \cdot \begin{pmatrix} 1 & 0 \\ 0 & -ie^{-i\lambda-i\phi_2} \end{pmatrix} \cdot \begin{pmatrix} \cos(\frac{\theta_1}{2}) & \sin(\frac{\theta_1}{2}) e^{-i\phi_1} \\ -\sin(\frac{\theta_1}{2}) e^{i\phi_1} & \cos(\frac{\theta_1}{2}) \end{pmatrix} \quad (88)$$

The parameters of the starting position in Eqn. 9 are expressed as:

$$\cos\left(\frac{\mu}{2}\right) = |\beta| = \sqrt{(Re(\beta))^2 + (Im(\beta))^2}, \quad (89)$$

$$\nu = \arctan\left(\frac{Im(\gamma)}{Re(\gamma)}\right) - \arctan\left(\frac{Im(\beta)}{Re(\beta)}\right), \quad (90)$$

with σ , and λ parameters given by the Eqns. 91, 92, 93, and 94 as:

$$\cos(\sigma) = \sqrt{\frac{1 + \cos(\theta_1) \cos(\theta_2) + \sin(\theta_1) \sin(\theta_2) \cos(\phi_1 - \phi_2)}{2}}, \quad (91)$$

$$\lambda = \arctan \left(\frac{\sin \left(\frac{\theta_1}{2} \right) \cos \left(\frac{\theta_2}{2} \right) \sin (\phi_2 - \phi_1)}{\cos \left(\frac{\theta_1}{2} \right) \sin \left(\frac{\theta_2}{2} \right) - \sin \left(\frac{\theta_1}{2} \right) \cos \left(\frac{\theta_2}{2} \right) \cos (\phi_2 - \phi_1)} \right) - \arctan \left(\frac{\sin \left(\frac{\theta_1}{2} \right) \sin \left(\frac{\theta_2}{2} \right) \sin (\phi_2 - \phi_1)}{\cos \left(\frac{\theta_1}{2} \right) \cos \left(\frac{\theta_2}{2} \right) + \sin \left(\frac{\theta_1}{2} \right) \sin \left(\frac{\theta_2}{2} \right) \cos (\phi_2 - \phi_1)} \right), \quad (92)$$

$$\beta = \cos \left(\frac{\theta_1}{2} \right) \cos \left(\frac{\theta_3}{2} \right) \cos \left(\frac{\pi - 2\sigma}{4} \right) \left(1 + \tan \left(\frac{\theta_1}{2} \right) \tan \left(\frac{\pi - 2\sigma}{4} \right) e^{i\phi_1 - i\phi_2 - i\lambda} \right) + \sin \left(\frac{\theta_1}{2} \right) \sin \left(\frac{\theta_3}{2} \right) \cos \left(\frac{\pi - 2\sigma}{4} \right) e^{i\phi_3 - i\phi_1} \left(1 - \cot \left(\frac{\theta_1}{2} \right) \tan \left(\frac{\pi - 2\sigma}{4} \right) e^{i\phi_1 - i\phi_2 - i\lambda} \right), \quad (93)$$

$$\gamma = i \cos \left(\frac{\theta_1}{2} \right) \cos \left(\frac{\theta_3}{2} \right) \sin \left(\frac{\pi - 2\sigma}{4} \right) \left(\tan \left(\frac{\theta_1}{2} \right) \cot \left(\frac{\pi - 2\sigma}{4} \right) e^{i\phi_1 - i\phi_2 - i\lambda} - 1 \right) - i \sin \left(\frac{\theta_1}{2} \right) \sin \left(\frac{\theta_3}{2} \right) \sin \left(\frac{\pi - 2\sigma}{4} \right) e^{i\phi_3 - i\phi_1} \left(1 + \cot \left(\frac{\theta_1}{2} \right) \cot \left(\frac{\pi - 2\sigma}{4} \right) e^{i\phi_1 - i\phi_2 - i\lambda} \right) \quad (94)$$

Unitary rotation, *Step 2*

The unitary rotation adjusting the states into the starting positions for the *Step 3* and the second \mathcal{PT} -symmetric evolution has the following parameters:

$$\kappa = \cos \left(\frac{\mu}{2} \right) \left(\cos (\omega\tau - \alpha) \cos \left(\frac{\delta}{2} \right) + \sin (\omega\tau) \sin \left(\frac{\delta}{2} \right) \right) + i e^{i\nu} \sin \left(\frac{\mu}{2} \right) \left(\cos (\omega\tau + \alpha) \sin \left(\frac{\delta}{2} \right) - \sin (\omega\tau) \cos \left(\frac{\delta}{2} \right) \right), \quad (95)$$

$$\zeta = i \cos \left(\frac{\mu}{2} \right) \left(\cos (\omega\tau - \alpha) \sin \left(\frac{\delta}{2} \right) - \sin (\omega\tau) \cos \left(\frac{\delta}{2} \right) \right) + e^{i\nu} \sin \left(\frac{\mu}{2} \right) \left(\cos (\omega\tau + \alpha) \cos \left(\frac{\delta}{2} \right) + \sin (\omega\tau) \sin \left(\frac{\delta}{2} \right) \right), \quad (96)$$

$$\cos \left(\frac{\xi}{2} \right) = \frac{|\kappa|}{\sqrt{|\kappa|^2 + |\zeta|^2}}, \quad \chi = \arctan \left(\frac{\text{Im}(\zeta)}{\text{Re}(\zeta)} \right) - \arctan \left(\frac{\text{Im}(\kappa)}{\text{Re}(\kappa)} \right) \quad (97)$$

Implementation of \mathcal{PT} symmetry by the dilation method

The combined qubit-ancilla system is governed by the following *Hermitian* Hamiltonian:

$$H_{a,q}^{Total}(t) = \hat{1} \otimes \Sigma(t) + \sigma_y \otimes \Upsilon(t), \quad (98)$$

and its elements are given by:

$$\Sigma(t) = \left[\mathcal{H}_q(t) + i \frac{d\zeta(t)}{dt} \zeta(t) + \zeta(t) \mathcal{H}_q(t) \zeta(t) \right] \mathcal{N}^{-1}(t), \quad (99)$$

$$\Upsilon(t) = i \left[\mathcal{H}_q(t) \zeta(t) - \zeta(t) \mathcal{H}_q(t) - i \frac{d\zeta(t)}{dt} \right] \mathcal{N}^{-1}(t), \quad (100)$$

$$\mathcal{N}(t) = T \exp \left[-i \int_0^t d\tau \mathcal{H}_q^\dagger(\tau) \right] \mathcal{N}(0) \tilde{T} \exp \left[i \int_0^t d\tau \mathcal{H}(\tau) \right], \quad (101)$$

where T and \tilde{T} are the time and anti-time-ordering operators, respectively. The operator $\zeta(t) = (\mathcal{N}(t) - \hat{1})^{\frac{1}{2}}$ must maintain all its eigenvalues to be real, and the initial value $\mathcal{N}(0)$ must be correspondingly chosen to ensure it. The following system of equations:

$$\begin{cases} \Sigma(t) - i\Upsilon(t) \zeta(t) = \mathcal{H}_q(t) \\ \Sigma(t) \zeta(t) + i\Upsilon(t) = i \frac{d\zeta(t)}{dt} + \zeta(t) \mathcal{H}_q(t) \end{cases}, \quad (102)$$

ensures that the driven qubit is evolved by the \mathcal{PT} -symmetric Hamiltonian in Eqn. 2. The ancilla qubit must be initialized as $|\psi(0)\rangle_a = \frac{1}{\sqrt{\zeta(0)^2+1}} (|0\rangle_a + \zeta(0) |1\rangle_a)$. For both stages of the \mathcal{PT} -symmetric evolution, 4×4 evolution matrix was obtained by numerical solution of differential equations by Mathematica [99]. Finally, the evolution matrices $U_{Evolution}$ were decomposed into the elementary gates U3 as defined by IBM. For the first part of the \mathcal{PT} -symmetric evolution, they are denoted as U_j^i , and V_j^i for the second part, where $i, j \in [1, 4]$. This was done employing the method defined in [100, 101]. First, the rotation to the “magic basis” defined as:

$$\begin{cases} |\phi_1\rangle = \frac{1}{\sqrt{2}} (|00\rangle + |11\rangle); & |\phi_2\rangle = \frac{-i}{\sqrt{2}} (|00\rangle - |11\rangle) \\ |\phi_3\rangle = \frac{1}{\sqrt{2}} (|01\rangle - |10\rangle); & |\phi_4\rangle = \frac{-i}{\sqrt{2}} (|01\rangle + |10\rangle) \end{cases}, \quad (103)$$

was performed. As a result, the evolution matrix was factorized as:

$$U_{Evolution} = (U_A \otimes U_B) \cdot U_D \cdot (V_A \otimes V_B), \quad (104)$$

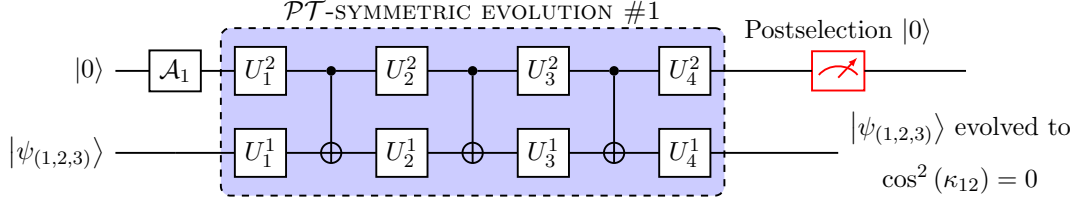


Figure 19. *Step 1* and the first stage of the \mathcal{PT} -symmetric evolution.

$$U_D = e^{i\theta_0} \text{MatrixExp} \left(i \sum_{k=1}^3 \theta_k \sigma_k \otimes \sigma_k \right) = \sum_{k=1}^4 e^{i\Phi_k} |\phi_k\rangle \langle \phi_k| \quad (105)$$

The final transformation is carried out by M and Λ matrices:

$$M = \frac{1}{\sqrt{2}} \begin{pmatrix} 1 & 0 & 0 & i \\ 0 & i & 1 & 1 \\ 0 & i & -1 & 0 \\ 1 & 0 & 0 & -i \end{pmatrix}, \quad \Lambda = \begin{pmatrix} 1 & 1 & -1 & 1 \\ 1 & 1 & 1 & -1 \\ 1 & -1 & -1 & -1 \\ 1 & -1 & 1 & 1 \end{pmatrix}, \quad (106)$$

$$\theta = (\theta_0, \theta_1, \theta_2, \theta_3)^T; \quad \Phi = (\Phi_0, \Phi_1, \Phi_2, \Phi_3)^T; \quad \theta = \Lambda \cdot \Phi \quad (107)$$

The numerical results are as follows.

1. *First \mathcal{PT} -symmetric evolution for $\sigma = \frac{4}{5}$, $\alpha = \frac{\pi}{2} - 1$, $\mathcal{N}(0) = 3$*

$U^{\text{FirstStage}} =$

$$\begin{bmatrix} 0.142552 - 0.235663i & -0.650522 - 0.393504i & 0.2897 - 0.478919i & -0.155267 - 0.0939248i \\ -0.650482 - 0.393478i & 0.257979 - 0.426478i & -0.155257 - 0.0939158i & -0.194071 + 0.320825i \\ -0.289696 + 0.478909i & 0.155284 + 0.0939324i & 0.142546 - 0.23565i & -0.650547 - 0.393515i \\ 0.15525 + 0.0939129i & 0.194076 - 0.320837i & -0.650472 - 0.393474i & 0.257971 - 0.42646i \end{bmatrix}$$

$$(\Phi_0, \Phi_1, \Phi_2, \Phi_3) = (1.61364, 1.61364, 2.61598, 2.61598), \quad (108)$$

$$U_A = \begin{pmatrix} 0.553173 - 0.0868701i & 0.128532 + 0.818494i \\ 0.818494 - 0.128536i & -0.0868671 - 0.553173i \end{pmatrix}, \quad (109)$$

$$U_B = \begin{pmatrix} 0.27538 - 0.495893i & 0.823563 \\ 0.252434 - 0.783922i & -0.556431 + 0.110127i \end{pmatrix}, \quad (110)$$

$$V_A = \begin{pmatrix} -0.35228i & -0.9359i \\ -0.9359 & 0.35228 \end{pmatrix}, \quad (111)$$

$$V_B = \begin{pmatrix} 0.1277 - 0.81357i & 0.19514 - 0.53266i \\ 0.53266 - 0.19514i & -0.81357 + 0.1277i \end{pmatrix} \quad (112)$$

2. *First \mathcal{PT} -symmetric Evolution for $\sigma = \frac{6}{5}$, $\alpha = \frac{\pi}{2} - 1$, $\mathcal{N}(0) = 2$*

$U^{\text{FirstStage}} =$

$$\begin{bmatrix} 0.49542 - 0.32066i & -0.28774 - 0.44456i & 0.50219 - 0.32504i & -0.06318 - 0.09762i \\ -0.28768 - 0.44447i & 0.66023 - 0.42733i & -0.06317 - 0.0976i & -0.24838 + 0.16076i \\ -0.50223 + 0.32506i & 0.06318 + 0.09761i & 0.49546 - 0.32069i & -0.28773 - 0.44455i \\ 0.06318 + 0.09762i & 0.24838 - 0.16076i & -0.28769 - 0.44449i & 0.66024 - 0.42733i \end{bmatrix}$$

$$(\Phi_0, \Phi_1, \Phi_2, \Phi_3) = (-0.09904, -0.09904, -1.04982, -1.04984), \quad (113)$$

$$U_A = \begin{pmatrix} 0.32195 + 0.35488i & -0.65003 + 0.5898i \\ 0.58977 + 0.65006i & 0.35485 - 0.32198i \end{pmatrix}, \quad (114)$$

$$U_B = \begin{pmatrix} -0.68589 + 0.4424i & 0.57779 \\ -0.57506 + 0.05604i & -0.72556 - 0.37379i \end{pmatrix}, \quad (115)$$

$$V_A = \begin{pmatrix} 0. & -0.27972i & -0.00004 - 0.96008i \\ -0.96008 - 0.00002i & 0.27972 & \end{pmatrix}, \quad (116)$$

$$V_B = \begin{pmatrix} -0.42795 - 0.38828i & -0.78849 - 0.21068i \\ 0.21067 + 0.78849i & -0.38827 - 0.42795i \end{pmatrix} \quad (117)$$

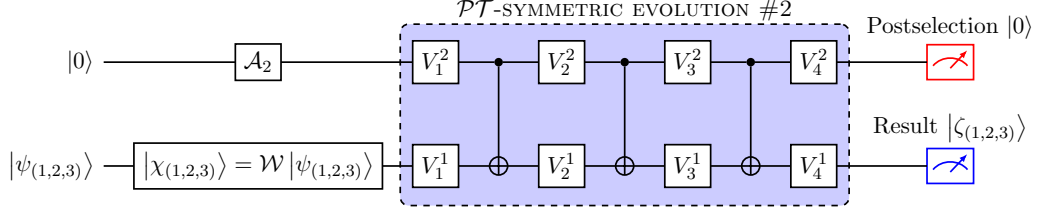


Figure 20. *Steps 2 and 3.* Unitary rotation \mathcal{W} puts the evolved state into conventional positions, and the second \mathcal{PT} -symmetric evolution eliminates one of three states or reduces them to the mirror-symmetric ones.

3. *Second \mathcal{PT} -symmetric Evolution, $\alpha = \frac{\pi}{2} - 1$*

$$U^{\text{Second stage}} = \begin{pmatrix} 0.20775i & -0.75471 & 0.55429i & 0.28286 \\ -0.75471 & -0.2077i & 0.28292 & -0.55429i \\ -0.55429i & -0.28286 & 0.20775i & -0.75471 \\ -0.28292 & 0.55429i & -0.75471 & -0.2077i \end{pmatrix} \quad (118)$$

$$U_A = \begin{pmatrix} -0.35523 - 0.0003i & -0.94791 - 0.00081i \\ 0.94791 + 0.00081i & -0.35523 - 0.0003i \end{pmatrix}, \quad (119)$$

$$U_B = \begin{pmatrix} 0.00085 - i & 0.00005 \\ -0.00005 & -0.00085 + i \end{pmatrix}, \quad (120)$$

$$V_A = V_B = \hat{1}; (\Phi_0, \Phi_1, \Phi_2, \Phi_3) = (0.93734, -0.93734, 0.93734, -0.93734) \quad (121)$$

4. *Second \mathcal{PT} -symmetric Evolution, $\alpha = \frac{\pi}{2} - 0.7$*

$$U^{\text{Second stage}} = \begin{pmatrix} 0.29118i & -0.68017 & 0.57944i & 0.3418 \\ -0.68017 & -0.29097i & 0.34196 & -0.57945i \\ -0.57944i & -0.3418 & 0.29118i & -0.68017 \\ -0.34197 & 0.57946i & -0.68016 & -0.29098i \end{pmatrix} \quad (122)$$

$$U_A = \begin{pmatrix} -0.44888 - 0.00094i & -0.89359 - 0.00187i \\ 0.89359 + 0.00187i & -0.44888 - 0.00094i \end{pmatrix}, \quad (123)$$

$$U_B = \begin{pmatrix} -0.0021 - i & 0.00011 \\ -0.00011 & 0.0021 + i \end{pmatrix}, \quad (124)$$

$$V_A = V_B = \hat{1}; (\Phi_0, \Phi_1, \Phi_2, \Phi_3) = (0.86525, -0.86525, 0.86525, -0.86525) \quad (125)$$

5. *Second \mathcal{PT} -symmetric Evolution, $\alpha = \frac{\pi}{2} - 0.5$*

$$U^{\text{Second stage}} = \begin{pmatrix} 0.3604i & -0.62104 & 0.5786i & 0.38684 \\ -0.6211 & -0.36067i & 0.3866 & -0.57852i \\ -0.5786i & -0.38684 & 0.36039i & -0.62105 \\ -0.3866 & 0.57852i & -0.62111 & -0.36067i \end{pmatrix} \quad (126)$$

$$U_A = \begin{pmatrix} 0.52887 & 0.8487 + 0.00001i \\ -0.8487 - 0.00001i & 0.52887 \end{pmatrix}, \quad (127)$$

$$U_B = \begin{pmatrix} 0.00001 + i & 0.00017 \\ -0.00017 & -0.00001 - i \end{pmatrix}, \quad (128)$$

$$V_A = V_B = \hat{1}; (\Phi_0, \Phi_1, \Phi_2, \Phi_3) = (0.82071, -0.82071, 0.82071, -0.82072) \quad (129)$$

The first part of the \mathcal{PT} -symmetric evolution is shown in Fig. 19, and the unitary rotation with the second part of the \mathcal{PT} -symmetric evolution in Fig. 20 respectively.

6. *Attack on the three-state QKD protocol*

$$U^{\text{Three State QKD}} = \begin{pmatrix} -0.09739i & -0.87214 & 0.43866i & -0.1937 \\ -0.87215 & 0.0974i & -0.19372 & -0.43864i \\ -0.4386i & 0.19367 & -0.09744i & -0.87212 \\ 0.19366 & 0.43861i & -0.8721 & 0.09742i \end{pmatrix} \quad (130)$$

$$U_A = \begin{pmatrix} -0.2167 + 0.00644i & 0.97579 - 0.02899i \\ -0.97579 + 0.02899i & -0.2167 + 0.00644i \end{pmatrix}, \quad (131)$$

$$U_B = \begin{pmatrix} -0.02969 + 0.99956i & 0.00001 \\ -0.00001 & 0.02969 - 0.99956i \end{pmatrix}, \quad (132)$$

$$V_A = V_B = \hat{1}; (\Phi_0, \Phi_1, \Phi_2, \Phi_3) = (1.10479, -1.10479, 1.10482, -1.10482) \quad (133)$$

- [1] J. A. Bergou, *Discrimination of quantum states*, *Journal of Modern Optics*, vol. 57, no. 3, pp. 160–180, 2010, Taylor & Francis.
- [2] C. W. Helstrom, *Quantum detection and estimation theory*, vol. 84, 1976, Academic press New York.
- [3] S. M. Barnett and S. Croke, *Quantum state discrimination*, *Advances in Optics and Photonics*, vol. 1, no. 2, pp. 238–278, 2009, Optical Society of America.
- [4] A. Chefles, *Quantum state discrimination*, *Contemporary Physics*, vol. 41, no. 6, pp. 401–424, 2000, Taylor & Francis.
- [5] S. P. Gudder and others, *Probabilistic and statistical aspects of quantum theory*, *Bulletin (New Series) of the American Mathematical Society*, vol. 13, no. 1, pp. 80–85, 1985, American Mathematical Society.
- [6] Joonwoo Bae, Leong-Chuan Kwek, *Quantum state discrimination and its applications*, *Journal of Physics A: Mathematical and Theoretical*, vol. 48, no. 8, p. 083001, 2015, IOP Publishing.
- [7] K. M. R. Audenaert, J. Calsamiglia, R. Muñoz-Tapia, E. Bagan, L. Masanes, A. Acín, and F. Verstraete, *Discriminating states: The quantum Chernoff bound*, *Physical Review Letters*, vol. 98, no. 16, p. 160501, 2007, APS.
- [8] N. Brunner, M. Navascués, and T. Vértesi, *Dimension witnesses and quantum state discrimination*, *Physical Review Letters*, vol. 110, no. 15, p. 150501, 2013, APS.
- [9] R. König, R. Renner, and C. Schaffner, *The operational meaning of min- and max-entropy*, *IEEE Transactions on Information Theory*, vol. 55, no. 9, pp. 4337–4347, 2009, IEEE.

- [10] William K. Wootters, Wojciech H. Zurek, *A single quantum cannot be cloned*, *Nature*, vol. 299, no. 5886, pp. 802–803, 1982, Nature Publishing Group.
- [11] Daniel S Abrams, Seth Lloyd, *Nonlinear quantum mechanics implies polynomial-time solution for NP-complete and #P problems*, *Physical Review Letters*, vol. 81, no. 18, p. 3992, 1998, APS.
- [12] D. Dieks, *Overlap and distinguishability of quantum states*, *Physics Letters A*, vol. 126, no. 5-6, pp. 303–306, 1988, Elsevier.
- [13] I. D. Ivanovic, *How to differentiate between non-orthogonal states*, *Physics Letters A*, vol. 123, no. 6, pp. 257–259, 1987, Elsevier.
- [14] S. Croke, E. Andersson, S. M. Barnett, C. R. Gilson, and J. Jeffers, *Maximum confidence quantum measurements*, *Physical Review Letters*, vol. 96, no. 7, p. 070401, 2006, APS.
- [15] Y. C. Eldar, A. Megretski, and G. C. Verghese, *Optimal detection of symmetric mixed quantum states*, *IEEE Transactions on Information Theory*, vol. 50, no. 6, pp. 1198–1207, 2004, IEEE.
- [16] E. Andersson, S. M. Barnett, C. R. Gilson, and K. Hunter, *Minimum-error discrimination between three mirror-symmetric states*, *Physical Review A*, vol. 65, no. 5, p. 052308, 2002, APS.
- [17] K. Hunter, *Results in optimal discrimination*, *AIP Conference Proceedings*, vol. 734, no. 1, pp. 83–86, 2004, American Institute of Physics.
- [18] B. F. Samsonov, *Minimum error discrimination problem for pure qubit states*, *Physical Review A*, vol. 80, no. 5, p. 052305, 2009, APS.
- [19] M. A. Jafarizadeh, *Minimum-error discrimination between two sets of similarity-transformed quantum states*, *arXiv preprint arXiv:1106.5883*, 2011.
- [20] D. Ha and Y. Kwon, *Complete analysis for three-qubit mixed-state discrimination*, *Physical Review A*, vol. 87, no. 6, p. 062302, 2013, APS.
- [21] A. Chefles, *Unambiguous discrimination between linearly independent quantum states*, *Physics Letters A*, vol. 239, no. 6, pp. 339–347, 1998, Elsevier.
- [22] Carl M. Bender, Dorje C. Brody, Hugh F. Jones, *Complex extension of quantum mechanics*, *Physical Review Letters*, vol. 89, no. 27, p. 270401, 2002, APS.

- [23] Carl M. Bender, Dorje C. Brody, Hugh F. Jones, *Must a Hamiltonian be Hermitian?*, *American Journal of Physics*, vol. 71, no. 11, pp. 1095–1102, 2003, American Association of Physics Teachers.
- [24] Ali Mostafazadeh, *Pseudo-Hermiticity versus PT -symmetry III: Equivalence of pseudo-Hermiticity and the presence of antilinear symmetries*, *Journal of Mathematical Physics*, vol. 43, no. 8, pp. 3944–3951, 2002, American Institute of Physics.
- [25] C. M. Bender, P. N. Meisinger, and Q. Wang, *Finite-dimensional PT -symmetric Hamiltonians*, *Journal of Physics A: Mathematical and General*, vol. 36, no. 24, p. 6791, 2003, IOP Publishing.
- [26] Ş. K. Özdemir, S. Rotter, F. Nori, and L. Yang, *Parity–time symmetry and exceptional points in photonics*, *Nature materials*, vol. 18, no. 8, pp. 783–798, 2019, Nature Publishing Group.
- [27] M.-A. Miri and A. Alu, *Exceptional points in optics and photonics*, *Science*, vol. 363, no. 6422, 2019, American Association for the Advancement of Science.
- [28] Carl M Bender, Dorje C Brody, Hugh F Jones, Bernhard K Meister, *Faster than Hermitian quantum mechanics*, *Physical Review Letters*, vol. 98, no. 4, p. 040403, 2007, APS.
- [29] Chao Zheng, Liang Hao, Gui Lu Long, *Observation of a fast evolution in a parity-time-symmetric system*, *Philosophical Transactions of the Royal Society A: Mathematical, Physical and Engineering Sciences*, vol. 371, no. 1989, p. 20120053, 2013, The Royal Society Publishing.
- [30] M. Zhang, W. Sweeney, C. W. Hsu, L. Yang, A. D. Stone, and L. Jiang, *Quantum noise theory of exceptional point amplifying sensors*, *Physical review letters*, vol. 123, no. 18, p. 180501, 2019, APS.
- [31] H.-K. Lau and A. A. Clerk, *Fundamental limits and non-reciprocal approaches in non-Hermitian quantum sensing*, *Nature communications*, vol. 9, no. 1, p. 1–13, 2018, Nature Publishing Group.
- [32] W. Langbein, *No exceptional precision of exceptional-point sensors*, *Physical Review A*, vol. 98, no. 2, p. 023805, 2018, APS.
- [33] H. Hodaei, A. U. Hassan, S. Wittek, H. Garcia-Gracia, R. El-Ganainy, D. N. Christodoulides, and M. Khajavikhan, *Enhanced sensitivity at higher-order exceptional points*, *Nature*, vol. 548,

- no. 7666, pp. 187–191, 2017, Nature Publishing Group.
- [34] W. Chen, Ş. K. Özdemir, G. Zhao, J. Wiersig, and L. Yang, *Exceptional points enhance sensing in an optical microcavity*, *Nature*, vol. 548, no. 7666, pp. 192–196, 2017, Nature Publishing Group.
- [35] J. Wiersig, *Enhancing the sensitivity of frequency and energy splitting detection by using exceptional points: application to microcavity sensors for single-particle detection*, *Physical Review Letters*, vol. 112, no. 20, p. 203901, 2014, APS.
- [36] Shang Yu, Yu Meng, Jian-Shun Tang, Xiao-Ye Xu, Yi-Tao Wang, Peng Yin, Zhi-Jin Ke, Wei Liu, Zhi-Peng Li, Yuan-Ze Yang, and others, *Experimental Investigation of Quantum PT -Enhanced Sensor*, *Physical Review Letters*, vol. 125, no. 24, p. 240506, 2020, APS.
- [37] You-neng Guo, Mao-fa Fang, Guo-you Wang, Jiang Hang, Ke Zeng, *Enhancing parameter estimation precision by non-Hermitian operator process*, *Quantum Information Processing*, vol. 16, no. 12, pp. 1–13, 2017, Springer.
- [38] Yan-Yi Wang and Mao-Fa Fang, *Quantum Fisher information of a two-level system controlled by non-Hermitian operation under depolarization*, *Quantum Information Processing*, vol. 19, no. 6, pp. 1–11, 2020, Springer.
- [39] Y. Balytskyi, M. Raavi, A. Pinchuk, and S. Y. Chang, *Detecting bias in randomness by PT -symmetric quantum state discrimination*, in *ICC 2021-IEEE International Conference on Communications*, pp. 1–6, 2021, IEEE.
- [40] Y. Balytskyi, M. Raavi, Y. Kotukh, and S.-Y. Chang, *PT -symmetric Bayesian parameter estimation on a superconducting quantum processor*, *ICC 2022-IEEE International Conference on Communications*, pp. 1–6, 2022, IEEE.
- [41] Y. Balytskyi, M. Raavi, and S.-Y. Chang, *PT -enhanced Bayesian parameter estimation*, *QCE 2021-IEEE International Conference on Quantum Computing and Engineering*, 2021, IEEE.
- [42] M. Partanen, J. Goetz, K. Y. Tan, K. Kohvakka, V. Sevriuk, R. E. Lake, R. Kokkonen, J. Ikonen, D. Hazra, A. Mäkinen, and others, *Exceptional points in tunable superconducting resonators*, *Physical Review B*, vol. 100, no. 13, p. 134505, 2019, APS.
- [43] J. Li, A. K. Harter, J. Liu, L. de Melo, Y. N. Joglekar, and L. Luo, *Observation of parity-time symmetry breaking transitions in a dissipative Floquet system of ultracold atoms*, *Nature*

- communications*, vol. 10, no. 1, pp. 1–7, 2019, Nature Publishing Group.
- [44] X. Zhu, H. Ramezani, C. Shi, J. Zhu, and X. Zhang, *PT-symmetric acoustics*, *Physical Review X*, vol. 4, no. 3, p. 031042, 2014, APS.
- [45] C. Shi, M. Dubois, Y. Chen, L. Cheng, H. Ramezani, Y. Wang, and X. Zhang, *Accessing the exceptional points of parity-time symmetric acoustics*, *Nature communications*, vol. 7, no. 1, pp. 1–5, 2016, Nature Publishing Group.
- [46] C. M. Bender, B. K. Berntson, D. Parker, and E. Samuel, *Observation of PT phase transition in a simple mechanical system*, *American Journal of Physics*, vol. 81, no. 3, pp. 173–179, 2013, American Association of Physics Teachers.
- [47] J. Schindler, Z. Lin, J. M. Lee, H. Ramezani, F. M. Ellis, and T. Kottos, *-symmetric electronics*, *Journal of Physics A: Mathematical and Theoretical*, vol. 45, no. 44, p. 444029, 2012, IOP Publishing.
- [48] B. Peng, Ş. K. Özdemir, F. Lei, F. Monifi, M. Gianfreda, G. Lu Long, S. Fan, F. Nori, C. M. Bender, and L. Yang, *Parity–time–symmetric whispering-gallery microcavities*, *Nature Physics*, vol. 10, no. 5, pp. 394–398, 2014, Nature Publishing Group.
- [49] C. E. Rüter, K. G. Makris, R. El-Ganainy, D. N. Christodoulides, M. Segev, and D. Kip, *Observation of parity–time symmetry in optics*, *Nature physics*, vol. 6, no. 3, pp. 192–195, 2010, Nature Publishing Group.
- [50] C. Dembowski, H.-D. Gräf, H. L. Harney, A. Heine, W. D. Heiss, H. Rehfeld, and A. Richter, *Experimental observation of the topological structure of exceptional points*, *Physical review letters*, vol. 86, no. 5, p. 787, 2001, APS.
- [51] Z. J. Wong, Y.-L. Xu, J. Kim, K. O’Brien, Y. Wang, L. Feng, and X. Zhang, *Lasing and anti-lasing in a single cavity*, *Nature Photonics*, vol. 10, no. 12, pp. 796–801, 2016, Nature Publishing Group.
- [52] M. Brandstetter, M. Liertzer, C. Deutsch, P. Klang, J. Schöberl, H. E. Türeci, G. Strasser, K. Unterrainer, and S. Rotter, *Reversing the pump dependence of a laser at an exceptional point*, *Nature communications*, vol. 5, no. 1, pp. 1–7, 2014, Nature Publishing Group.
- [53] B. Peng, Ş. K. Özdemir, M. Liertzer, W. Chen, J. Kramer, H. Yılmaz, J. Wiersig, S. Rotter, and L. Yang, *Chiral modes and directional lasing at exceptional points*, *Proceedings of the*

- National Academy of Sciences*, vol. 113, no. 25, pp. 6845–6850, 2016, National Acad Sciences.
- [54] X.-L. Zhang, S. Wang, B. Hou, and C. T. Chan, *Dynamically encircling exceptional points: in situ control of encircling loops and the role of the starting point*, *Physical Review X*, vol. 8, no. 2, p. 021066, 2018, APS.
- [55] Y. Choi, C. Hahn, J. W. Yoon, S. H. Song, and P. Berini, *Extremely broadband, on-chip optical nonreciprocity enabled by mimicking nonlinear anti-adiabatic quantum jumps near exceptional points*, *Nature communications*, vol. 8, no. 1, p. 1–9, 2017, Nature Publishing Group.
- [56] J. Doppler, A. A. Mailybaev, J. Böhm, U. Kuhl, A. Girschik, F. Libisch, T. J. Milburn, P. Rabl, N. Moiseyev, and S. Rotter, *Dynamically encircling an exceptional point for asymmetric mode switching*, *Nature*, vol. 537, no. 7618, p. 76–79, 2016, Nature Publishing Group.
- [57] H. Xu, D. Mason, L. Jiang, and J. G. E. Harris, *Topological energy transfer in an optomechanical system with exceptional points*, *Nature*, vol. 537, no. 7618, p. 80–83, 2016, Nature Publishing Group.
- [58] Carl M Bender, Dorje C Brody, João Caldeira, Uwe Günther, Bernhard K Meister, Boris F Samsonov, *PT-symmetric quantum state discrimination*, *Philosophical Transactions of the Royal Society A: Mathematical, Physical and Engineering Sciences*, vol. 371, no. 1989, p. 20120160, 2013, The Royal Society Publishing.
- [59] Yaroslav Balytskyi, Manohar Raavi, Anatoliy Pinchuk, Sang-Yoon Chang, *PT-Symmetric Quantum Discrimination of Three States*, *arXiv preprint arXiv:2012.14897*, 2020.
- [60] Dong-Xu Chen, Yu Zhang, Jun-Long Zhao, Qi-Cheng Wu, Yu-Liang Fang, Chui-Ping Yang, Franco Nori, *Quantum state discrimination in a PT-symmetric system*, *Physical Review A*, vol. 106, no. 2, p. 022438, 2022, APS.
- [61] Yang Wu, Wenquan Liu, Jianpei Geng, Xingrui Song, Xiangyu Ye, Chang-Kui Duan, Xing Rong, Jiangfeng Du, *Observation of parity-time symmetry breaking in a single-spin system*, *Science*, vol. 364, no. 6443, pp. 878–880, 2019, American Association for the Advancement of Science.
- [62] Shruti Dogra, Artem A. Melnikov, Gheorghe Sorin Paroanu, *Quantum simulation of parity-time symmetry breaking with a superconducting quantum processor*, *Communications Physics*, vol. 4, no. 1, pp. 1–8, 2021, Nature Publishing Group.

- [63] Patrick Dorey, Clare Dunning, Roberto Tateo, *Spectral equivalences, Bethe ansatz equations, and reality properties in PT -symmetric quantum mechanics*, *Journal of Physics A: Mathematical and General*, vol. 34, no. 28, p. 5679, 2001, IOP Publishing.
- [64] Patrick Dorey, Clare Dunning, Roberto Tateo, *A reality proof in PT -symmetric quantum mechanics*, *Czechoslovak Journal of Physics*, vol. 54, no. 1, pp. 35–41, 2004, Springer.
- [65] Daniel Gottesman, *Stabilizer codes and quantum error correction*, California Institute of Technology, 1997.
- [66] M. A. Neumark, *Izv. Akad. SSSR Ser. Mat.* **4**, 1940.
- [67] A. Kandala, K. Temme, A. D. Córcoles, A. Mezzacapo, J. M. Chow, and J. M. Gambetta, *Error mitigation extends the computational reach of a noisy quantum processor*, *Nature*, vol. 567, no. 7749, pp. 491–495, 2019, Nature Publishing Group.
- [68] H.-L. Huang, D. Wu, D. Fan, and X. Zhu, *Superconducting quantum computing: a review*, *Science China Information Sciences*, vol. 63, no. 8, pp. 1–32, 2020, Springer.
- [69] S. J. Devitt, *Performing quantum computing experiments in the cloud*, *Physical Review A*, vol. 94, no. 3, p. 032329, 2016, APS.
- [70] R. Harper and S. T. Flammia, *Fault-tolerant logical gates in the ibm quantum experience*, *Physical review letters*, vol. 122, no. 8, p. 080504, 2019, APS.
- [71] D. Alsina and J. I. Latorre, *Experimental test of Mermin inequalities on a five-qubit quantum computer*, *Physical Review A*, vol. 94, no. 1, p. 012314, 2016, APS.
- [72] E. Huffman and A. Mizel, *Violation of noninvasive macrorealism by a superconducting qubit: Implementation of a Leggett-Garg test that addresses the clumsiness loophole*, *Physical Review A*, vol. 95, no. 3, p. 032131, 2017, APS.
- [73] N. N. Hegade, A. Das, S. Seth, and P. K. Panigrahi, *Investigation of quantum pigeonhole effect in IBM quantum computer*, *arXiv preprint arXiv:1904.12187*, 2019.
- [74] G. S. Paraoanu, *Non-local parity measurements and the quantum pigeonhole effect*, *Entropy*, vol. 20, no. 8, p. 606, 2018, Multidisciplinary Digital Publishing Institute.
- [75] G. García-Pérez, M. A. C. Rossi, and S. Maniscalco, *IBM Q Experience as a versatile experimental testbed for simulating open quantum systems*, *npj Quantum Information*, vol. 6, no. 1, pp. 1–10, 2020, Nature Publishing Group.

- [76] Y. Wang, Y. Li, Z.-q. Yin, and B. Zeng, *16-qubit IBM universal quantum computer can be fully entangled*, *npj Quantum information*, vol. 4, no. 1, pp. 1–6, 2018, Nature Publishing Group.
- [77] A. Kandala, A. Mezzacapo, K. Temme, M. Takita, M. Brink, J. M. Chow, and J. M. Gambetta, *Hardware-efficient variational quantum eigensolver for small molecules and quantum magnets*, *Nature*, vol. 549, no. 7671, pp. 242–246, 2017, Nature Publishing Group.
- [78] H.-Y. Ku, N. Lambert, F.-J. Chan, C. Emary, Y.-N. Chen, and F. Nori, *Experimental test of non-macrorealistic cat states in the cloud*, *npj Quantum Information*, vol. 6, no. 1, pp. 1–9, 2020, Nature Publishing Group.
- [79] S.-L. Chen, G.-Y. Chen, and Y.-N. Chen, *Increase of entanglement by local PT -symmetric operations*, *Physical Review A*, vol. 90, no. 5, p. 054301, 2014, APS.
- [80] S. J. D. Phoenix, S. M. Barnett, and A. Chefles, *Three-state quantum cryptography*, *Journal of modern optics*, vol. 47, no. 2-3, pp. 507–516, 2000, Taylor & Francis.
- [81] D. Poulin, *Stabilizer formalism for operator quantum error correction*, *Physical Review Letters*, vol. 95, no. 23, p. 230504, 2005, APS.
- [82] B. M. Terhal, *Quantum error correction for quantum memories*, *Reviews of Modern Physics*, vol. 87, no. 2, p. 307, 2015, APS.
- [83] J. Combes, C. Ferrie, Z. Jiang, and C. M. Caves, *Quantum limits on postselected, probabilistic quantum metrology*, *Physical Review A*, vol. 89, no. 5, p. 052117, 2014, APS.
- [84] Y. Chu, Y. Liu, H. Liu, and J. Cai, *Quantum sensing with a single-qubit pseudo-Hermitian system*, *Physical Review Letters*, vol. 124, no. 2, p. 020501, 2020, APS.
- [85] Wenkui Ding, Xiaoguang Wang, Shu Chen, *Fundamental Sensitivity Limits for non-Hermitian Quantum Sensors*, *Physical Review Letters*, vol. 131, 160801, 2023, APS.
- [86] A. N. Jordan, J. Martínez-Rincón, and J. C. Howell, *Technical advantages for weak-value amplification: when less is more*, *Physical Review X*, vol. 4, no. 1, p. 011031, 2014, APS.
- [87] J. Preskill, *Quantum computing in the NISQ era and beyond*, *Quantum*, vol. 2, p. 79, 2018, Verein zur Förderung des Open Access Publizierens in den Quantenwissenschaften.
- [88] O. Ezratty, *Where are we heading with NISQ?*, *arXiv preprint arXiv:2305.09518*, 2023.
- [89] G. Alagic et al., *Status report on the third round of the NIST post-quantum cryptography*

- standardization process, US Department of Commerce, NIST, 2022.*
- [90] National Institute of Standards and Technology, *Submission Requirements and Evaluation Criteria for the Post-Quantum Cryptography Standardization Process*, 2016, Available at <https://csrc.nist.gov/CSRC/media/Projects/Post-QuantumCryptography/documents/call-for-proposals-final-dec-2016.pdf>.
 - [91] P. W. Shor, *Algorithms for quantum computation: discrete logarithms and factoring*, in *Proceedings 35th Annual Symposium on Foundations of Computer Science*, pp. 124–134, 1994, IEEE.
 - [92] P. W. Shor, *Polynomial-time algorithms for prime factorization and discrete logarithms on a quantum computer*, *SIAM Review*, vol. 41, no. 2, pp. 303–332, 1999, SIAM.
 - [93] L. K. Grover, *Proceedings of the twenty-eighth annual ACM symposium on Theory of computing, STOC'96*, pp. 212–219, 1996, Association for Computing Machinery New York.
 - [94] C. Zalka, *Grover's quantum searching algorithm is optimal*, *Physical Review A*, vol. 60, no. 4, p. 2746, 1999, APS.
 - [95] S. Croke, *PT-symmetric Hamiltonians and their application in quantum information*, *Physical Review A*, vol. 91, no. 5, p. 052113, 2015, APS.
 - [96] K. Zhang and V. E. Korepin, *Depth optimization of quantum search algorithms beyond Grover's algorithm*, *Physical Review A*, vol. 101, no. 3, p. 032346, 2020, APS.
 - [97] R. M. Gingrich, C. P. Williams, and N. J. Cerf, *Generalized quantum search with parallelism*, *Physical Review A*, vol. 61, no. 5, p. 052313, 2000, APS.
 - [98] O. Regev and L. Schiff, *Impossibility of a quantum speed-up with a faulty oracle*, in *International Colloquium on Automata, Languages, and Programming*, pp. 773–781, 2008, Springer.
 - [99] *Wolfram Mathematica software*, <https://www.wolfram.com/mathematica/>.
 - [100] P. B. M. Sousa and R. V. Ramos, *Universal quantum circuit for n-qubit quantum gate: A programmable quantum gate*, *arXiv preprint quant-ph/0602174*, 2006.
 - [101] F. Vatan and C. Williams, *Optimal quantum circuits for general two-qubit gates*, *Physical Review A*, vol. 69, no. 3, p. 032315, 2004, APS.